ADVANCED OPTICAL MATERIALS
www.advopticalmat.de

# Engineering Optical Absorption in Graphene and Other 2D Materials: Advances and Applications

*Qiang Li,* Jun Lu,* Prince Gupta, and Min Qiu*

**2D materials are promising but remain to be further explored, with respect to their usage in various optoelectronic devices. Generally, 2D materials exhibit far less than ideal absorption due to their thickness, limiting their deployment in practical optoelectronic applications. To address this challenge, extensive research has been performed utilizing different designs, such as distributed Bragg reflector microcavities, metallic reflectors, photonic crystal nanocavities, and plasmonic nanostructures, to confine light within 2D materials and increase light absorption. Recent progresses in enhancing light absorption in graphene and other 2D materials such as transition metal dichalcogenides and phosphorene are reviewed. Some physical mechanisms that realize enhanced absorption in 2D materials, as well as their potential applications are also discussed.**

## 1. Introduction

Two-dimensional (2D) materials are crystalline materials consisting of only single or few layers of atoms. Ever since the first exfoliation of graphene in 2004,[1] there have been significant efforts to study the unusual mechanical, electrical, and optical properties of graphene and other graphene-like 2D materials,[2,3] which find applications in numerous disciplines including optoelectronics,[4] photovoltaics,[5] materials, energy, and nanotechnology.[6] Currently, the most studied and promising 2D materials include graphene, transition metal dichalcogenides (TMDs, such as $MoS_2$, $MoSe_2$, $WSe_2$, and $WS_2$), phosphorene (i.e., monolayer of black phosphorus [BP]),[7] and hexagonal boron nitride (h-BN). These 2D materials exhibit diverse electrical and optical properties, which could lead to a variety of applications in electronics and optoelectronics. Graphene is a metal-like material with zero band gap and linear energy dispersion. TMDs have indirect band gaps (usually 1.2–1.4 eV) in bulk forms, but exhibit larger direct band gap (1.7–2.2 eV) when thinned down to monolayers.[8] BP has a direct band-gap (0.3 eV in bulk form, 2 eV in monolayer form[9]). Owing to their direct band gap in the near-infrared (NIR)-to-visible range, the TMD and BP monolayers are particularly promising with respect to their integration into optoelectronics devices. h-BN has a large band gap well above the visible range (≈6.0 eV[10]) and hence is more insulator-like and has a high transparency. The combinations of these 2D layers to create various van der Waals heterostructures with varying functionalities have also become a focus of attention.[11–13]

One of the most noteworthy features of the 2D materials is that despite being atomically thin, many 2D materials, including graphene, TMDs, and BP, interact with light strongly. For example, a one-atom thick single layer of graphene (with a thickness of ≈0.335 nm) can absorb 2.3%, and a monolayer $MoS_2$ (with a thickness of ≈0.615 nm) absorbs an average of ≈10% of incident visible light.[14] Such a strong light absorption is essential, but may still not be sufficient for the application in optoelectronic devices, for example, photodetectors and photovoltaic devices, which require higher absorbance in order to increase the power conversion efficiency.

The performance of 2D-material-based optoelectronic devices (e.g., responsivity, wavelength, bandwidth, response time, etc.) also depends on materials, structure designs, doping, contact engineering, and heterojunction formation.[15] In this review, we focus on the recent advancements in enhancement and control over the optical absorption in layers of graphene, TMDs, and BP in the infrared-to-visible range, as well as their applications in 2D-material-based devices. A brief introduction of the optical properties of the 2D materials and the design principle of light absorption is discussed in Section 2. Further, the progress of absorption enhancement in graphene (Section 3) and TMD and BP layers (Section 4) is presented and discussed. The control and tunability of absorption enhancements, and their potential applications are presented in Sections 5 and 6, respectively. Finally, we will outline the perspectives and challenges.

Prof. Q. Li, Dr. J. Lu, Dr. P. Gupta
State Key Laboratory of Modern Optical Instrumentation
College of Optical Science and Engineering
Zhejiang University
Hangzhou 310027, China
E-mail: qiangli@zju.edu.cn; phylujun@zju.edu.cn
Prof. M. Qiu
School of Engineering
Westlake University
18 Shilongshan Road, Hangzhou 310024, China
Prof. M. Qiu
Institute of Advanced Technology
Westlake Institute for Advanced Study
18 Shilongshan Road, Hangzhou 310024, China
The ORCID identification number(s) for the author(s) of this article can be found under https://doi.org/10.1002/adom.201900595.

**DOI: 10.1002/adom.201900595**

## 2. Optical Absorptions in 2D Materials

### 2.1. Intrinsic Absorption in 2D Materials

Graphene has a unique electronic structure in which the valence and conduction bands exactly intersect at the Dirac points (the K-points) (**Figure 1**a), resulting in a metal-like zero-gap material with a linear energy dispersion in the vicinity of these points.[16] It was found by Nair et al. that suspended graphene has a broadband and relatively high light absorption of 2.3%,[17] which is defined solely by the fine structure constant $\alpha$ ($\pi\alpha \approx 2.3\%$ in the infrared-to-visible region (below 3 eV). Moreover, the absorption scales linearly with the number of layers, that is, increases by another 2.3% with every additional layer (see Figure 1a). Another advantage is that the reflectance of graphene is negligible (<0.1%). The absorption coefficient is $\approx 6.8 \times 10^5$ cm$^{-1}$, which is quite large compared to that of 3D bulk crystals.

Optical conductivity and complex refractive index of exfoliated and chemical-vapor-deposition (CVD) grown graphene have been measured with various techniques (e.g., transmission and reflection spectroscopy,[18,19] ellipsometry,[20,21] and the attenuated total reflectance method[22,23]) and theoretically studied by ab initio calculations, such as density functional theory.[24–26] For pristine graphene, only interband transitions between the valance and conductance bands are possible, resulting in a universal surface conductivity $\sigma = e^2/4\hbar$[18,27] corresponding to an opacity of $Z_0\sigma = \pi\alpha \approx 2.3\%$, where $e$ is the elementary charge, $\hbar$ is the reduced Planck constant, and $Z_0$ ($= \sqrt{\mu_0/\varepsilon_0}$) is the vacuum impedance. Meanwhile, graphene can be easily doped by chemical doping and electrostatic gating. For doped graphene, both interband and intraband (free-carrier) transitions exist. The doping level and the transitions are attributable to the chemical potential $\mu_c$ (alternatively denoted as the Fermi level $E_F$), which induces Pauli blocking of interband transitions. As shown in **Figure 2**b, in longer wavelength regime where $\hbar\omega < 2\mu_c$, the optical conductivity is dominated by the intraband transition and thus can be well approximated by a Drude model. On the other hand, in the shorter infrared-to-visible regime (where the interband transition dominates), conductivity is nearly wavelength independent, except for the decreased conductivity and absorption in the vicinity of $\hbar\omega \gtrsim 2\mu_c$ due to Pauli blocking. In the NIR-to-visible range, the shifted Fermi level does not significantly affect the imaginary part of the dielectric function and hence the absorption spectra.[26] There is only a small increasement in the absorption by less than 1% due to a band filling effect.[25] In the ultraviolet range where the transitions reach the saddle-point singularity (the M-points, see Figure 2a), the absorption increases and exhibits significant excitonic effects.[28,29]

Considering the optical transitions near the K-points, the surface conductivity of monolayer graphene can be given by the Kubo formula.[30]

$$\sigma(\omega, \mu_c, \Gamma, T) = \sigma_{\text{intra}} + \sigma_{\text{inter}} \tag{1}$$

where

$$\sigma_{\text{intra}} = \frac{je^2}{\pi\hbar^2(\omega - j2\Gamma)} \int_{\xi=0}^{\infty} \xi df_d(\xi) - \xi df_d(-\xi) \tag{2}$$

**Qiang Li** is currently a professor at the College of Optical Science and Engineering, Zhejiang University. He received his B.Sc. and M.Eng. degrees from the Harbin Institute of Technology, China, and his Ph.D. degree in microelectronics and applied physics from the Royal Institute of Technology (KTH), Sweden. His research interests are focused on thermal photonics and their applications.

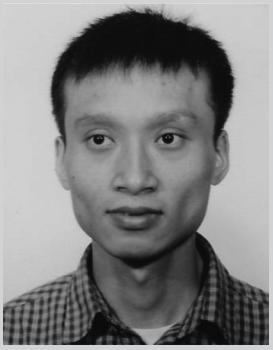

**Jun Lu** received his Ph.D. degree in physics from Zhejiang University, China, and is currently an associate professor at the College of Optical Science and Engineering, Zhejiang University. His research interest is in modeling and design of photonic devices.

**Min Qiu** received his Ph.D. degree in physics from Zhejiang University, China, and his second Ph.D. degree in electromagnetics from the Royal Institute of Technology (KTH), Sweden. He joined Westlake University (Hangzhou, China) as chair professor of photonics and vice president for research in 2018. Formerly he was a professor at Zhejiang University and KTH, and the director of the State Key Laboratory of Modern Optical Instrumentation, Zhejiang University. His research interests include nanofabrication technology, nanophotonics, and green photonics.

and

$$\sigma_{\text{inter}} = \frac{-je^2(\omega - j2\Gamma)}{\pi\hbar^2} \int_0^{\infty} \frac{f_d(-\xi) - f_d(\xi)}{(\omega - j2\Gamma)^2 - 4(\xi/\hbar)^2} d\xi \tag{3}$$

are conductivities due to intraband and interband distributions, respectively. $\Gamma$ represents the scattering rate, $T$ is the temperature, and

$$f_d(\xi) = \left(e^{\frac{\xi - \mu_c}{k_B T}} + 1\right)^{-1} \tag{4}$$

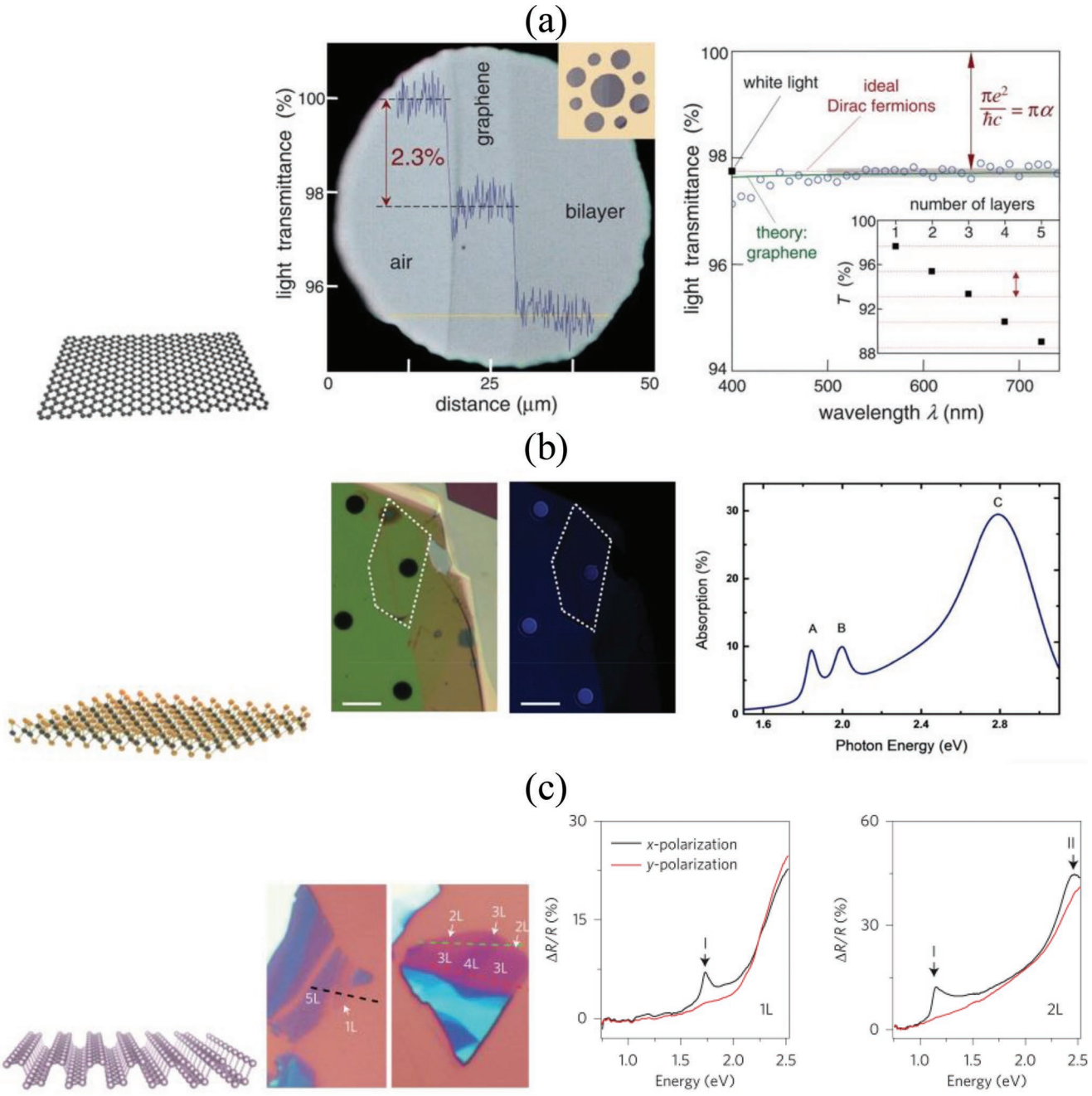


**Figure 1.** Optical absorption in 2D layers. a) Graphene. Adapted with permission.[17] Copyright 2008, American Association for the Advancement of Science. b) $MoS_2$. Adapted with permission.[39] Copyright 2015, IEEE. c) BP. Left: Adapted with permission.[46] Copyright 2014, Springer Nature. Right: Adapted with permission.[9] Copyright 2014, American Physical Society.

is the Fermi–Dirac distribution. $\Gamma$ and $\mu_c$ are related by $\Gamma = ev_F^2/2\mu\mu_c$,[31] where $v_F$ is the Fermi velocity ($\cong 1 \times 10^6$ m s$^{-1}$), and $\mu$ is the carrier mobility (typical values are ≈7000 cm$^2$ V$^{-1}$ s$^{-1}$ for graphene derived from CVD, and ≈10 000 cm$^2$ V$^{-1}$ s$^{-1}$ for mechanically exfoliated graphene).

Optical properties are also characterized using the volumetric permittivity $\varepsilon_r$ and the complex refractive index $n + ik$. Typical values of $n$, $k$, and $\varepsilon_r$ for monolayer graphene are shown Figure 2c. The complex refractive indices of monolayer $MoS_2$ and BP are presented in Figure 2d,e, respectively. The in-plane relative permittivity is related to the surface conductivity by

$$\varepsilon_{\parallel} = \varepsilon_r - j\frac{\sigma}{\varepsilon_0 \omega \Delta} \tag{5}$$

where $\varepsilon_r$ is the background relative permittivity where graphene resides, and $\Delta$ is the sheet thickness (≈0.335 nm for graphene). The out-of-plane relative permittivity is $\varepsilon_{\perp} = \varepsilon_r$ .

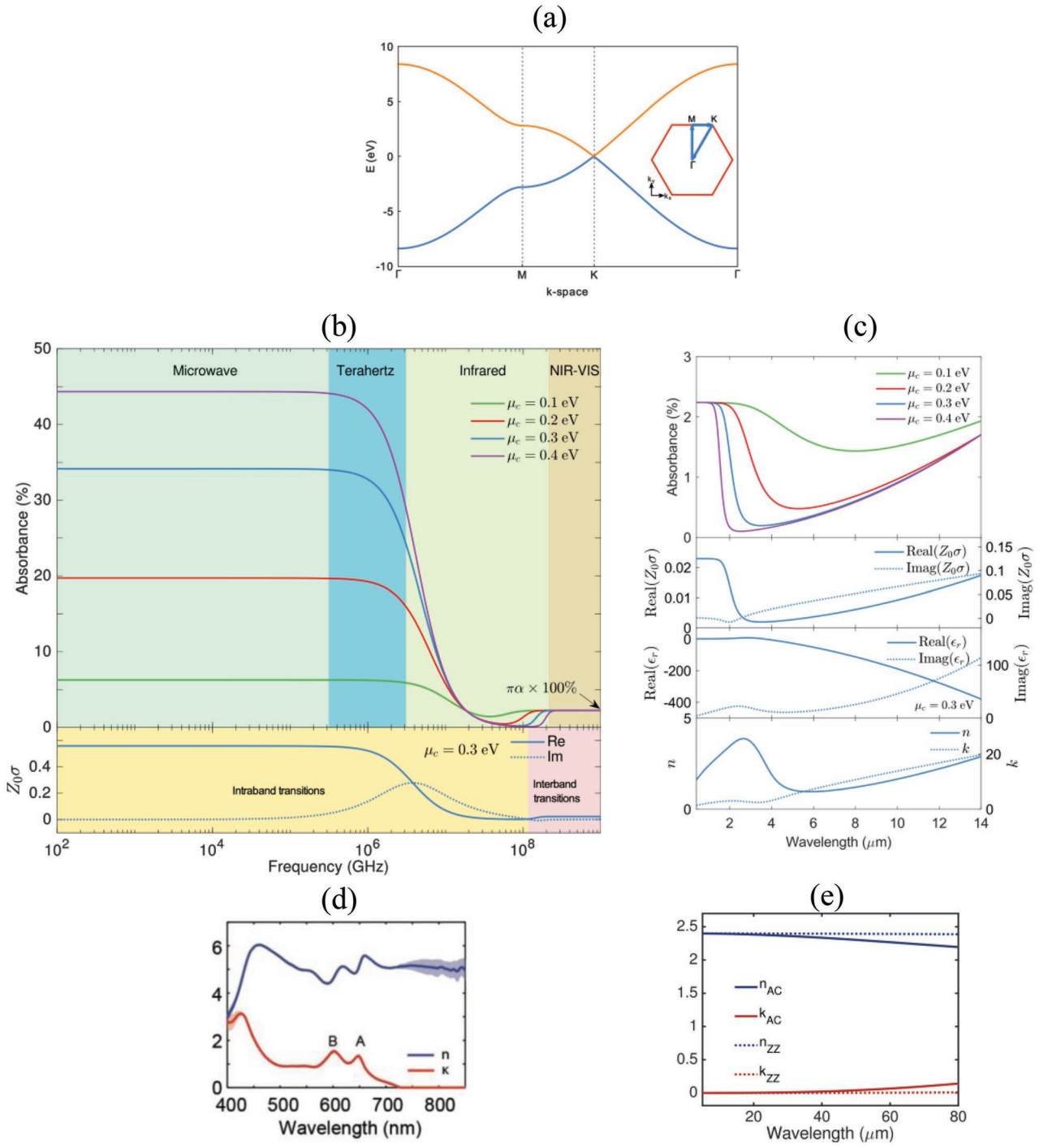


**Figure 2.** a) Band structure of a monolayer graphene along Γ-M-K-Γ in the Brillouin zone depicted as an insect. The linearly band structure near the K-points gives rise to many unique properties of graphene. b) Broadband absorption (upper) and surface conductivity (lower) of monolayer graphene sheets with different chemical potentials ( $\mu_c = 0.1$, 0.2, 0.3, and 0.4 eV). The lower blue solid and dotted lines are the real and imaginary parts of the conductivity, respectively, for $\mu_c = 0.3$ eV. c) Close-up of (b) for varying wavelengths in the infrared-to-visible range, together with the corresponding complex permittivity $\varepsilon_r$ and refractive index $n + ik$. d) Complex refractive index of monolayer $MoS_2$. Adapted with permission.[122] Copyright 2019, Wiley-VCH. e) Complex refractive index of monolayer $MoS_2$.

For a 2D thin film embedded between two semi-infinite dielectrics 1 and 3, the reflection ($r$) and transmission ($t$) coefficients of a plane wave normally incident from dielectric 1 are given by[32,33]

$$r = \frac{n_1 - n_3 - Z_0\sigma}{n_1 + n_3 + Z_0\sigma} \tag{6}$$

and

$$t = \frac{2n_1}{n_1 + n_3 + Z_0\sigma} \tag{7}$$

where the vacuum impedance $Z_0 = 1/\varepsilon_0 c$ . The absorption ($A$) is defined as

$$A = 1 - |r|^2 - \frac{n_3}{n_1}|t|^2 \tag{8}$$

For a standalone thin film in free space ( $n_1 = n_3 = 1$), Equation (8) becomes

$$A = \frac{4Z_0\sigma'}{(2 + Z_0\sigma')^2 + (Z_0\sigma'')^2} \tag{9}$$

where $\sigma'$ and $\sigma''$ are the real and imaginary parts of the surface conductivity $\sigma$, respectively. Figure 2b shows the surface conductivity and absorbance of monolayer graphene calculated using Equations (1) and (9) with the following parameters: $\mu$ = 7000 cm$^2$ V$^{-1}$ s$^{-1}$, $T$ = 300 K, and $\mu_c$ = 0.1, 0.2, 0.3, and 0.4 eV, respectively. Note that in the microwave region, the absorption of graphene can be easily controlled by chemical or electrical doping, as shown in Figure 2b. Graphene-based radar-absorbing surfaces have been experimentally realized to control the absorption of microwaves.[34] In the IR-to-terahertz (THz) region, the intraband transitions enable surface plasmons, resulting in enhanced electric field at nanometric dimension that can be used to enhance optical absorption.[35,36] In the NIR-to-visible region where interband transition dominates, surface plasmons are not present. The enhancement of absorption is achieved by use of optical resonators in this region, and will be addressed in Section 2.2 in detail.

Contrary to bulk TMD crystals, whose band gaps are still indirect even down to a thickness of two monolayers, some monolayer TMDs, for example, Mo- and W-based dichalcogenides, exhibit direct band gaps at the K-point of the Brillouin zone.[37] This makes them promising candidates for optoelectronic devices. Compared to graphene, TMD monolayers exhibit even higher absorption in the NIR-to-visible range, due to the excitonic coupling of transitions. Optical characteristics of TMD layers (including $MoS_2$, $MoSe_2$, $WS_2$, and $WSe_2$) were measured,[38–40] which exhibit strong optical absorption (see Figure 1b for monolayer $MoS_2$). This strong absorption by TMD layer is attributed to band nesting and corresponding divergence of joint density of states.[38] The lowest two peaks, labeled as A and B in Figures 1b and 2d correspond to excitons generated from the two spin-orbit split transitions at the K-point. The Peak A (at 690 nm) and Peak B (at 630 nm) have 10% absorption while another peak (at 450 nm) has 30% absorption.

BP is a direct band-gap semiconductor and exhibits a unique puckered honeycomb lattice structure. Spectral and polarization dependence of optical properties of few-layer BP was studied theoretically[9,41] and experimentally.[42–46] Due to its puckered structure the absorption shows strong dichroism, within a wide wavelength range (including infrared and part of visible light) few-layer BP absorbs light polarized along the armchair direction and is transparent to light polarized along the zigzag direction. This polarization-dependent behavior is more apparent in thicker layers. Li et al.[46] measured absorption of phosphorene encapsulated between h-BN layer and sapphire substrate. The absorption is highly layer-dependent due to layer–layer interactions, as the direct band gap varies from 1.73 eV in monolayer, 1.15 eV in bilayer, and 0.83 eV in trilayer BP to 0.35 eV in the bulk.

### 2.2. Design Principle for Absorption Enhancement

The basic principle to enhance absorption in thin films is to reduce reflection and transmission of light waves from the thin absorption layer. This can be generally done by introducing optical resonance to generate enhanced local electromagnetic fields (or to increase the overall optical path length) in the absorption layer. For a linear and isotropic absorption layer, the dissipation power per unit square/volume, $q$, is simply related to the local electric field intensity by $q = \frac{1}{2}\sigma'(\omega)|E(\omega)|^2$,[47] where $\sigma'$ is the real part of surface/volume optical conductivity, and $E$ is the electric field intensity. In such a scenario, an absorber can be modeled as a coupled resonator. According to the coupled mode theory (CMT),[48–50] the evolution equation for a single resonance coupled to a one-sided incident waves (see **Figure 3**a) can be written as

$$\frac{da}{dt} = \left(j\omega_0 - \gamma_0 - \gamma_1 - \gamma_2\right)a + \kappa_1 s_{1+} + \kappa_2 \cdot 0 \tag{10}$$

where $\omega_0$ is the resonant frequency of the resonant mode, $\gamma_0$ is the nonradiative decay rate describing internal losses of the mode, $\gamma_1$ and $\gamma_2$ are the decay rates describing the backward and forward radiations, respectively, $s_{1+}$ denotes the incoming wave, $\kappa_1$ and $\kappa_2$ are the coupling coefficients. The CMT model is illustrated in Figure 3a. Due to power conservation, $\kappa_i$ and $\gamma_i$ are related as $\kappa_i = \sqrt{2\gamma_i}$, ($i$ = 1,2). The absorptivity ($A$) is defined as

$$A = 1 - \left|\frac{s_{1-}}{s_{1+}}\right|^2 - \left|\frac{s_{2-}}{s_{1+}}\right|^2 \tag{11}$$

where $s_{1-} = e^{-j\beta d}(-s_{1+} + \kappa_1 a)$ and $s_{2-} = e^{-j\beta d}\kappa_2 a$ are the reflected and transmitted waves with $e^{-j\beta d}$ being the phase shift in the thin-film absorber, respectively. Solving Equations (10) and (11) yields a Lorentzian profile of absorption given as[51]

$$A = \frac{4\gamma_0\gamma_1}{(\omega - \omega_0)^2 + (\gamma_0 + \gamma_1 + \gamma_2)^2} \tag{12}$$

Equation (12) shows that the absorption can be maximized by matching the external radiative loss with the internal loss at the resonant frequency $\omega_0$. The absorption for varying external-to-internal decay-rate ratio is also shown in Figure 3c. In particular, in the case of a symmetric system ( $\gamma_1 = \gamma_2$ , e.g., thin-film structures in free space), the absorption can only reach a maximum of 50% at resonant frequency when $\gamma_1 = \gamma_2 = \gamma_0/2$. In the case of a one-port system (i.e., $\gamma_2 = 0$, the transmission of the resonator is blocked, e.g., by a perfect electrical conductor [PEC], see Figure 3b), total absorption occurs at resonant frequency when $\gamma_1 = \gamma_0$ (which is known as the critical coupling condition), with the full width at half maximum (FWHM) being reduced to $4\gamma_0$.

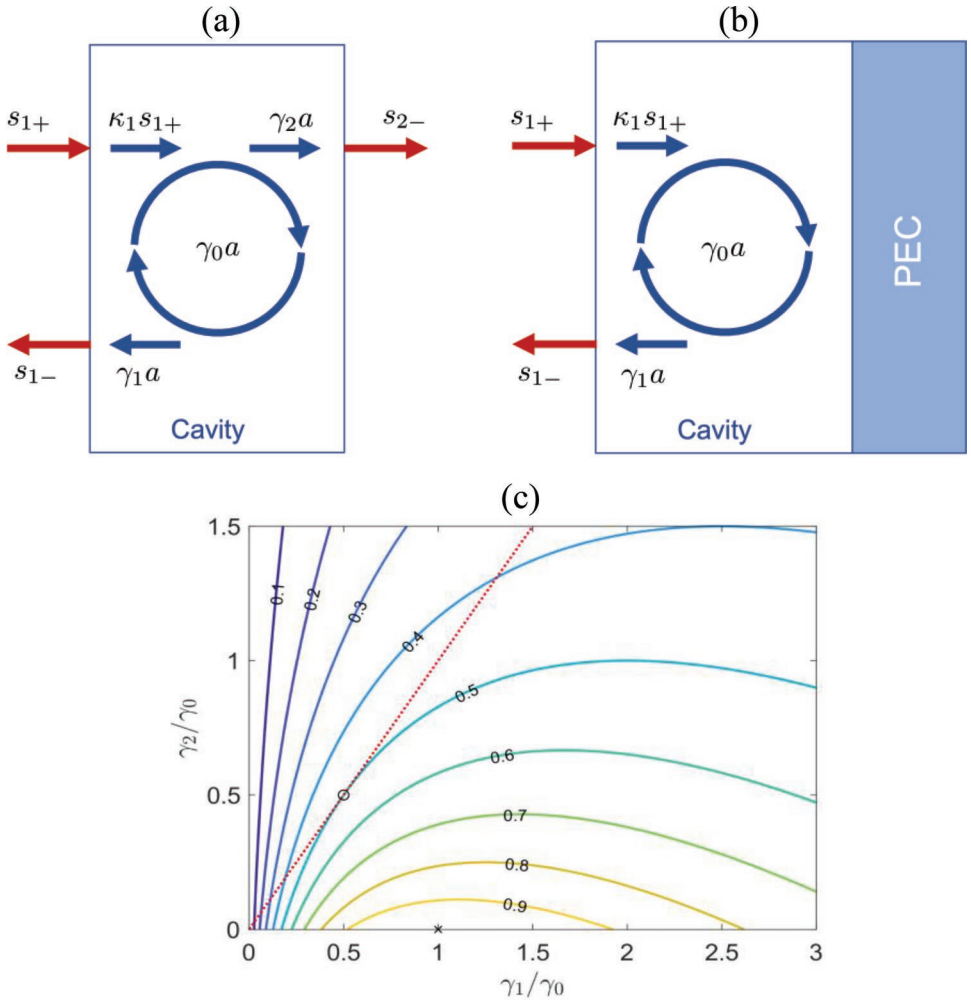


**Figure 3.** a) Schematic of absorption, reflection, and transmission of a thin-film resonator (Equation (10)). b) Schematic of absorption and reflection of a resonator back-terminated with a PEC mirror. c) Absorbance at resonant frequency $\omega_0$ versus varying backward and forward external-to-internal decay-rate ratio (Equation (12)). The red dotted line represents symmetric systems ( $\gamma_2 = \gamma_1$ ). The circled dot (o) represents the maximum absorption (50%) for symmetric systems. The cross dot (×) represents the maximum perfect absorption (100%) for resonators back-terminated with PEC mirror in (b) under critical coupling condition.

## 3. Enhancement of Absorption in Graphene

As shown by Equation (12), a lossy resonator can be used to create an enhanced but somewhat narrowband absorption. To enhance the absorption, a variety of optical resonators have been applied, for example, optical Salisbury screens (consisting of a single reflective mirror),[52] Fabry–Pérot cavities (consisting of double reflective mirrors),[53] guided resonances in photonic crystal slabs,[54–56] localized surface plasmon resonances,[57] and 2D-material plasmonic metasurfaces (i.e., patterned 2D-material layers).[35,36] In principle 100% absorption is possible as long as the transmission is blocked and the critical coupling condition is satisfied at the resonant frequency.

### 3.1. With a Single Mirror

The most straightforward way to enhance absorption in graphene is to place graphene sheets on reflective substrates that can create an antireflecting Salisbury screen effect. An ideal graphene Salisbury screen is formed by a monolayer graphene and a perfect reflective mirror sandwiched with a lossless dielectric spacer of a thickness of quarter wavelength. For such a system the internal and external decay rates at normal incidence are calculated as $\gamma_0 = Z_0\,\sigma' c/\varepsilon d$ and $\gamma_1 = c/\varepsilon d$ , respectively. From Equation (12), it can be easily approximated that the absorption has a maximum of $4Z_0\sigma'$ (i.e., four times the absorption of a standalone graphene) and an FWHM bandwidth of $2c/\varepsilon d$, provided that $Z_0\sigma' \approx 2.3\%$ for standalone graphene monolayer in the NIR-to-visible range. Liu et al.[58] theoretically demonstrated that the absorption of graphene can be enhanced fourfold (from 2.3% to 9% for monolayer graphene, and 24% for trilayer graphene at the wavelength of 550 nm) by separating the graphene sheet from a lossless Bragg reflector (also known as 1D photonic crystal) with a $SiO_2$ spacer layer (**Figure 4**a). The Bragg reflector is composed of alternating Si and $SiO_2$ layers with a total of 7.5 periods with a designed large photonic band gap across the visible region for normal incident light. Similarly,

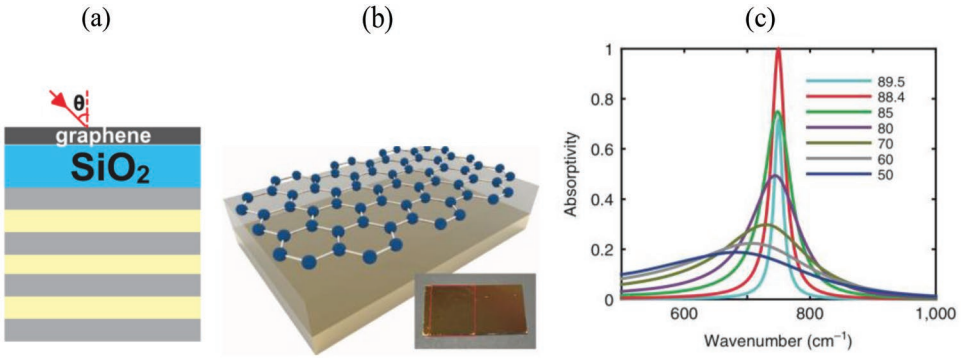


**Figure 4.** a,b) Schematic of two light absorbing structures consisting of a monolayer graphene, separated from (a) a distributed Bragg mirror, and (b) a perfect electric conductor mirror, respectively. c) Absorptance of the structure scheme in (b), for varying wavelengths and angles of incident. (a) Adapted with permission.[58] Copyright 2012, American Institute of Physics. (b,c) Adapted with permission.[52] Copyright 2016, Springer Nature.

the absorption of graphene can also be enhanced in terahertz (THz) range.[59] Liu et al.[60] further suggested the use of a metal film reflector in order to broaden the absorption spectrum. The metal film not only serves as a back reflector but also as a gate electrode, by which a gate voltage can be applied to modulate the Fermi level of graphene as well as the absorption of graphene in THz range. This leads to a structure consisting of a monolayer graphene separated from a metallic mirror by a dielectric spacer layer as shown in Figure 4b. At normal incidence, the enhancement is limited up to ≈fourfold due to the small value of $Z_0\sigma'$; however, Zhu et al.[52] argued that for such a simple structure, there exists a critical angle $\theta_c$, at which critical coupling with the resonance mode of the structure can be satisfied, and the absorptivity reaches unity. The value of $\theta_c$ can be calculated as follows

$$\theta_c = \frac{\pi}{2} - \frac{\varepsilon - 1}{\varepsilon}\pi\alpha \tag{13}$$

where $\varepsilon$ is the relative permittivity of the spacer layer. For a chemically doped monolayer graphene (with the Fermi energy $E_F = -500$ meV) placed on a structure consisting of a ≈1.9 µm-thick $Ge_{23}Sb_7S_{70}$ chalcogenide layer atop a 200-nm-thick gold mirror, the critical angle was calculated as $\theta_c \approx 88.4°$ (see Figure 4c). For an 89° angle of incidence, 47.2% absorption in graphene was experimentally achieved, along with 30.4% parasitic absorption in metal and spacer layers, which makes a total absorption of 77.6% in the mid-infrared wavelength range (≈13 µm). The absorption in graphene and the parasitic absorption were separated from experimental results using coupled mode theory.[52]

### 3.2. With Double Mirrors

It is also feasible to incorporate Fabry–Pérot interference to confine electromagnetic fields and enhance absorption.[61] The concept is simple, however, the integration of graphene with planar Fabry–Pérot cavities remains challenging. Furchi et al.[53] realized a graphene photodetector integrated with a Fabry–Pérot microcavity (**Figure 5**a), which can enhance the optical absorption up to 26-fold enhanced (>60%). The graphene layer is sandwiched between two distributed Bragg mirrors consisting of quarter-wavelength thick layers of alternating non-absorbing materials with varying refractive indices (seven pairs of $SiO_2$/$Si_3N_4$ layers for the top mirror, and 25 pairs of AlAs/$Al_{0.1}Ga_{0.9}As$ layers for the bottom mirror). Strong and spectrally narrow optical response with a FWHM of 9 nm was experimentally observed at the resonance wavelength of 855 nm (see Figure 5b). With such a designed microcavity, a graphene photodetector with a responsivity of 21 mA $W^{-1}$ was experimentally realized.

Another example of performing light confinement with double mirrors is using a metal film and a distributed dielectric Bragg mirror, as proposed and numerically studied by Lu et al.[62] The proposed structure consists of a graphene layer in a $SiO_2$ spacer layer, a top ultrathin metal layer, and a bottom alternately stacked $TiO_2$/$SiO_2$ layers, as shown in Figure 5c. The metal and Bragg mirrors form a surface wave confined in the $SiO_2$ spacer layer, resulting large absorption enhancement. The surface wave is so-called Tamm plasmon-polariton (TPP). The calculated total absorptivity of the structure and the absorptivity of the graphene layer, can reach 100% and 80%, respectively, at the resonance wavelength of 1553 nm with a spectral width of ≈17 nm (see Figure 5d).

### 3.3. With Photonic Crystal Nanocavities

In addition to using refractive mirrors the confinement of electromagnetic fields can also be done with photonic crystal (PC) nanocavities. Guided-mode resonance is a resonant effect in 1D and 2D PC slabs, which results from the out-of-plane excitation and radiation of in-plane guided modes through phase matching provided by the periodic structure. This provides another narrowband resonant light confinement mechanism. By integrating a monolayer graphene with a 1D PC slab, Rybin et al.[63] experimentally observed increased absorbance up to 16% at the resonance wavelength of 1590 nm with a bandwidth of 26.8 nm. The 1D PC guided-mode resonance reflector is formed from a three-layer Si/$SiO_2$ grating on SOI substrate, as shown in **Figure 6**a. The authors also predicted a maximum attainable absorbance of 50% via critical coupling of the absorption with the guided resonance in the reflector. A critical coupling design was realized by Liu et al.,[54] who experimentally obtained a peak absorption of 35% at 1545.5 nm with a FWHM of ≈4 nm from PC cavity coupled monolayer graphene, for a 2D Si resonance

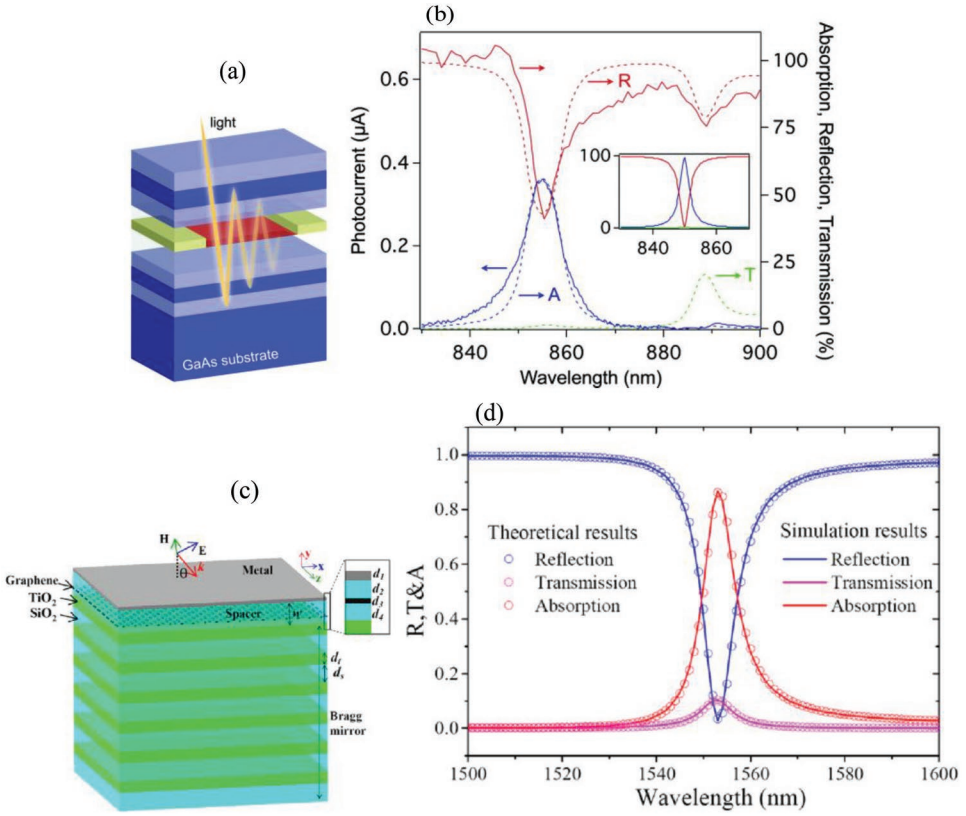


**Figure 5.** a) Schematic of a graphene microcavity composed of distributed Bragg mirrors. b) Spectral response of the single-layer graphene device. The dashed lines show calculation results: reflection R (red), transmission T (green), and absorption A (blue). (a,b) Adapted with permission.[53] Copyright 2012, American Chemical Society. c) Schematic of a structure consisting of a metal film coated on a Bragg mirror and a graphene sheet in a spacer. d) Spectral response of the structure scheme in (c). Strong absorption is due to the excitation of the TPP mode highly confined in the spacer. (c,d) Adapted with permission.[62] Copyright 2016, Optical Society of America.

PC structure (Figure 6c) without a back metal reflector and 85% for the case with Au thin film as the bask reflector (**Figure 7**c,d). Another example of exploiting guided-mode resonance was proposed by Grande et al.[64] This design shows a maximum attainable absorbance of ≈60% in theory and an experimental absorbance of 43% at 737 nm with the bandwidth of ≈7 nm for TE polarized light. The absorber is composed of a monolayer graphene sandwiched between a PMMA grating and a $Ta_2O_5$ slab supported by a $SiO_2$ substrate (see Figure 6e,f).

Additionally, Piper et al.[65] proposed a back-reflector-free total absorption scheme so-called degenerate critical coupling (Figure 6g). For a mirror-symmetric resonator, if the resonator supports two resonances that are degenerate in frequency but have opposite symmetry with respect to the mirror plane, total absorption will be attainable even without a back reflector when each resonance is critically coupled.[66] The numerical calculation shows an absorption spectrum with peak absorption of 98% at 1.32 μm and spectral width of 6 nm (see Figure 6h).[65]

### 3.4. With Photonic Crystal Nanocavities and Back Reflectors

It is well documented that by critical coupling to a guided resonance of a symmetric PC slab the maximum of absorption is 50%,[54,63,65,67] however, total absorption may be attainable by simply adding a perfect back reflector that makes the absorber a one-port system.[67] The perfect back reflector can be either a lossless metallic mirror or a multilayer dielectric Bragg mirror (Figure 7a,b). Experimentally the peak absorption increases from 35% to 85% by adding an Au-coated glass substrate to a Si PC slab (see Figure 7c,d).[54] Wang et al.[68] demonstrated a resonance PC structure, which shows 96% total absorption and 77% absorption in monolayer graphene at 1507 nm resonance wavelength with a bandwidth of ≈3 nm (Figure 7f). The proposed structure, as shown in Figure 7e, is composed of a 2D PC slab composed of $TiO_2$ cubes, a silver back reflector space from the PC slab by an $Al_2O_3$ spacer layer, and a monolayer graphene sandwiched between the PC slab and the $Al_2O_3$ layer.

1D and 2D PMMA PC slabs were also used to form resonances.[55,69,70] Grande et al.[55] numerically demonstrated that by adding a perfect mirror, perfect absorption over a bandwidth of few nanometers can be attained for a structure exploiting guide mode resonances. The proposed structure is composed of a 1D PMMA grating, a $Ta_2O_5$ slab grown on a $SiO_2$ substrate, an Au reflector spaced by the $SiO_2$ substrate, and a graphene layer sandwiched between the PMMA stripes and the $Ta_2O_5$ slab. Experimentally an absorption of about 37% near the wavelength of 735 nm was achieved. Guo et al.[69] proposed a similar structure comprising a monolayer graphene sandwiched between a 1D PMMA grating and a $SiO_2$ substrate back-coated

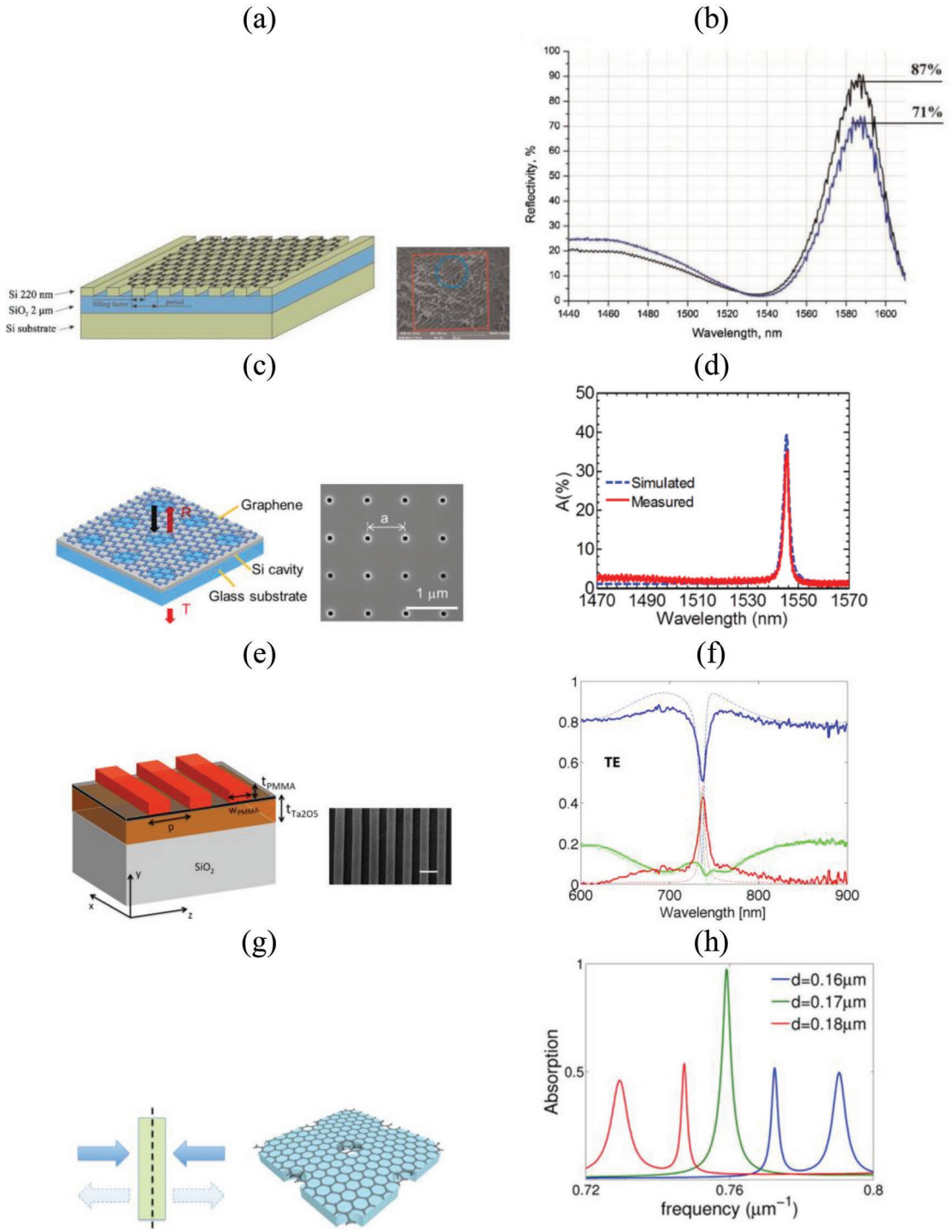


**Figure 6.** a,b) Schematic, SEM image, and reflectivity spectra of a reflective structure based on SOI substrate. The blue and black lines denote spectra without and with a monolayer graphene, respectively. Adapted with permission.[63] Copyright 2012, Wiley-VCH. c,d) Schematic, SEM image, and absorbance of a PC cavity structure. Adapted with permission.[54] Copyright 2014, AIP. e,f) Schematic, SEM image and transmittance (blue), reflectance (green), and absorbance (red) of a guided-mode resonance absorber. Adapted with permission.[64] Copyright 2014, OSA. g,h) Schematic and absorption enhancement blow, at and above the crossing of two resonances with opposite symmetry. The dashed line in (g) indicates the mirror plane symmetry of the system. Adapted with permission.[65] Copyright 2014, AIP.

with Au, showing nearly perfect absorption of 99% (89% in monolayer graphene and 11% in Au layer, respectively) at 1.5 μm wavelength with a FWHM of 20 nm for TE polarization (Figure 7g,h). Polarization-independent perfect absorption can be realized by replacing 1D gratings with 2D PC lattices (Figure 7i,j), as demonstrated by Fan et al.[70]

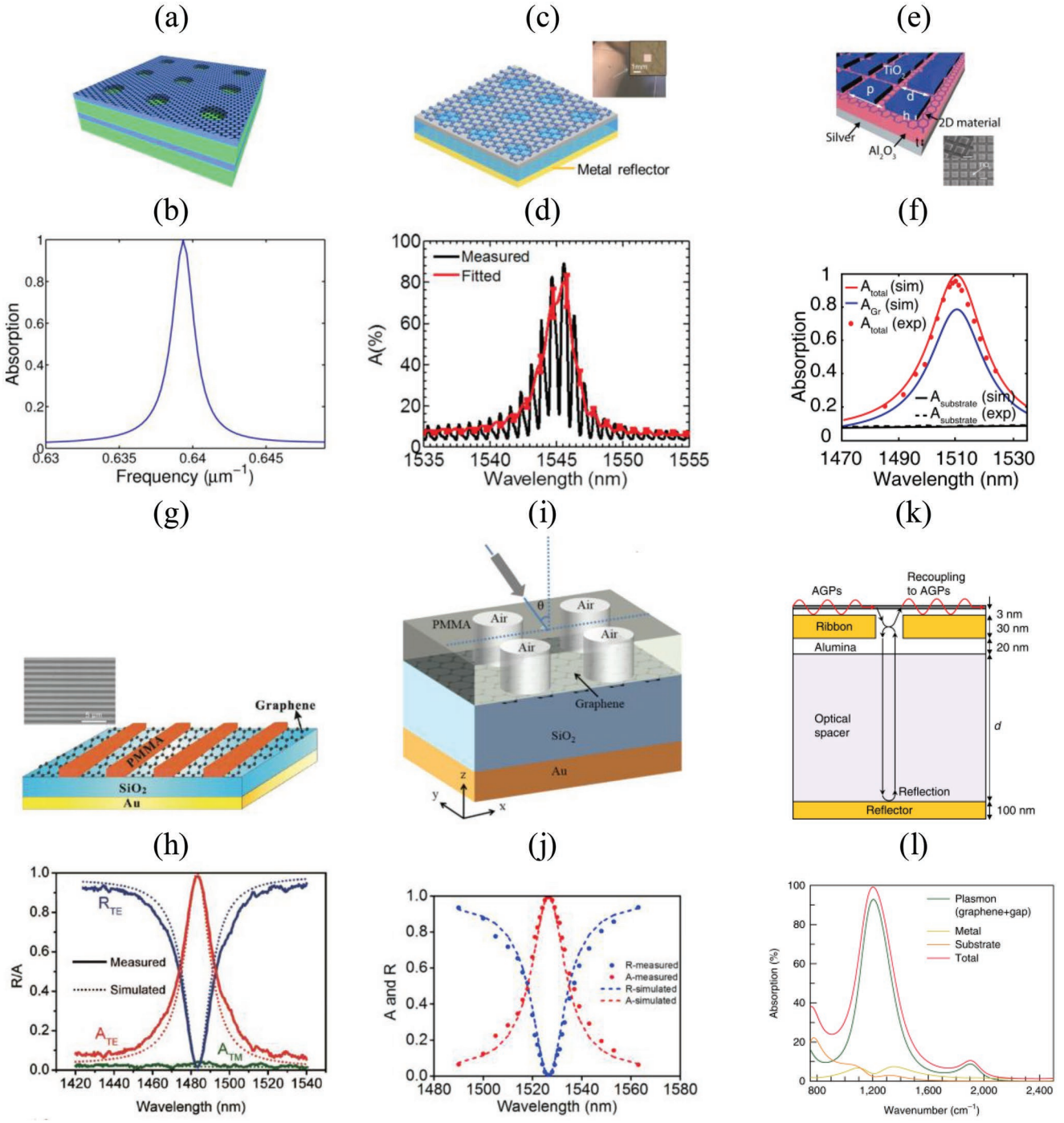


**Figure 7.** Schematics, images, and absorbance of structures with PC cavities backed with mirrors. a,b) Using a Bragg mirror.[2] Adapted with permission.[67] Copyright 2014, American Chemical Society. c,d) Using a metal reflector. The oscillate profile in (d) is due to the Fabry–Pérot associated with the finite glass substrate thickness. Adapted with permission.[54] Copyright 2014, AIP. e,f) 2D PC slab composed of $TiO_2$ cubes. Adapted with permission.[68] Copyright 2016, AIP. g,h) 1D PMMA grating. Adapted with permission.[69] Copyright 2017, OSA. i,j) 2D PMMA PC lattices. Adapted with permission.[70] Copyright 2017, OSA. k,l) Hybrid structure consisting of a graphene layer and an array of metal ribbons. Adapted with permission.[71] Copyright 2019, Springer Nature.

Strong enhancement of absorption in graphene can also be obtained when a graphene layer is combined with a patterned metal film to form an efficient light-confining plasmon resonator. Lu et al.[57] proposed a hybrid structure consisting of graphene layer on a metal film with an array of groove rings. The absorption peak appears near 1550 nm wavelength with 43.1% of incident light being absorbed by the graphene monolayer. Lee et al.[71] realized an acoustic graphene plasmon

resonator consisting of a monolayer graphene on a metal ribbon array separated by a nanogap (Figure 7k). The structure can achieve near perfect absorption, of which 94% is attributed plasmonic absorption in graphene (Figure 7l).

### 3.5. Periodically Patterned Graphene

Typically the maximum absorption by an unpatterned 2D material in a Salisbury screen configuration is about fourfold greater than the suspended or glass-supported monolayer.[58,72] However, this no longer holds true for ordered periodic plasmonic 2D structures, as doped graphene supports strongly confined surface plasmons in the THz and far-infrared. By use of patterned graphene structures, light-plasmon coupling in doped graphene has been experimentally explored.[73,74] For example, Yan et al.[73] fabricated a five-layer stacked graphene/insulator microdisk array, which is transparent in the NIR-to-visible but exhibits significant extinction ratio in the far-infrared region due to plasmonic resonance (see **Figure 8**a). In principle, total light absorption is possible via critical coupling for such periodic structures, as long as the absorption cross section of each unit cell comparably exceeds the area of the unit cell. By critically coupling free-space light into the nanoscale plasmonic resonances in the graphene structures, Thongrattanasiri et al.[35] theoretically predicted that a single sheet of doped graphene patterned into a periodic array of nanodisks, when the transmission channel is suppressed (e.g., under total internal reflection condition, or lying on a dielectric layer back-coated with a perfect metal) and under critical-coupling conditions, exhibits nearly 100% light absorption (Figure 8b). Experimental demonstration was performed by Fang et al.[36] (without the underlying metallic layer). By nanopatterning a graphene layer into an array of closely packed graphene nanodisks (of 60 nm in diameter and 90 nm in period), the absorbance of the structure (graphene on an In-$In_2O_3/BaF_2$ substrate, see Figure 8b) is voltage-tunable and can be increased up to 30% at about 6.9 μm with a spectral width of about 2 μm (Figure 8c). Also Jang et al.[75] demonstrated that by adjusting the size and carrier density of the patterned graphene plasmonic resonators, 24.5% total absorption is achieved in a patterned graphene sheet placed on a $SiN_x$ substrate with an Au back reflector. Kim et al.[76] experimentally introduced a 1D nanostructured graphene so called graphene plasmonic ribbons (see Figure 11c), which reaches 52.4% of absorption at about 7.14 μm with a Fermi level of–0.550 eV, when situated on a $SiO_2/SiN_x$ membrane with an Au back reflector. The enhanced absorption can be electrically tuned with a gate voltage (see Section 5).

**Table 1** summarizes the results from absorption enhancement of graphene described in this section. In particular, the structures employed for the enhancement, wavelengths, bandwidths, and magnitudes of absorption in the devices and by graphene layers, are listed for comparison.

## 4. Enhancement of Absorption in TMDs and Black Phosphorus

TMD and BP monolayers are new classes of 2D materials and have been extensively studied as 2D semiconductors. TMD layers exhibit larger and variable single-pass absorption in the visible light region due to excitonic coupling effects as compared to graphene. Similar to the case of graphene,[58,62] the absorbance of $MoS_2$ monolayer was theoretically calculated to be enhanced about fourfold (up to 35%) when incorporating a Salisbury screen type configuration,[72] and to be close to nearly perfect absorption (96%) when using a configuration consisting of a metal film, a dielectric grating, and an in-between spacer.[77] Instead of using critical coupling as the absorption-enhancement mechanism, which results in relatively narrowband absorption, Piper et al. proposed the use of multiple guided mode resonances supported by a thin photonic crystal slab with large air holes,[14] which results in broadband absorption enhancement over the entire frequency range above the band gap of $MoS_2$. With optimal design an average absorption of 51% can be attained. Experimentally Bahauddin et al.[78] reported a 3.9-fold enhanced broadband absorption of $MoS_2$ monolayer on a 40-nm-$Al_2O_3$/Al structure, compared to that of $MoS_2$ on a sapphire ($Al_2O_3$) structure. They also showed numerically that the average absorption of $MoS_2$ monolayer in Vis-NIR range can be further increased from 32% to 37% by incorporating Ag nanodisks below the $MoS_2$ monolayer (**Figure 9**a). Such a plasmonic enhanced broadband absorption was also demonstrated by depositing Au nanoparticles (with diameters of ≈150 nm) on $MoS_2$ monolayer on $SiO_2$/Si substrates,[79] increasing the absorption from nearly 8% to up to 41% (Figure 9b).

Based on a coupled leaky mode theory design, Huang et al.[56] proposed a critical coupling structure for narrowband perfect absorption, which consists of a $MoS_2$ film on top of a GaN nanowire array situated on an Ag-coated substrate (Figure 9c). They also suggested a broadband design composed of a GaN nanopillar array (on a sapphire substrate backed with a mirror) conformally coated with four-layer $MoS_2$ (Figure 9d). Strong absorption (>70%) can be realized for both the narrowband and broadband structures.

Unlike graphene (which is a gap-less material), enhanced absorption is also possible when TMDs, as 2D semiconductors, are in intimate contact with metals. Jariwala et al.[80] showed that an exfoliated $WSe_2$ film on an Au/Ag back reflecting substrate, when thicknesses of the film is between 12 and 15 nm, exhibits a broadband near-unity absorption (>90%) due to coupling to strongly damped optical modes of the van der Waals heterostructure (see Figure 9e). Also by simply spin-coating $MoS_2$ nanosheets onto an Au substrate, Zhang et al.[81] demonstrated a broadband, polarization-insensitive, near-perfect absorber whose absorption can reach more than 87% between 400 and 640 nm. The thickness of the $MoS_2$ layer is about 14 to 18 nm. The damping of incident waves can be further increased significantly by using plasmonic nanostructures and nanoantennas.[82,83] In particular, Eggleston et al.[83] demonstrated a 700-times photoluminescence (PL) enhancement in an etched nanostrip (30 nm × 250 nm) of monolayer $WSe_2$ coupled to an Ag cavity-backed slot antenna (Figure 9f). The large PL enhancement is partially due to increased optical absorption in the $WSe_2$ layer.

Monolayer BP is highly anisotropic due to its special puckered hexagonal lattice structure. Therefore, enhanced polarization-dependent and anisotropic absorption can be obtained

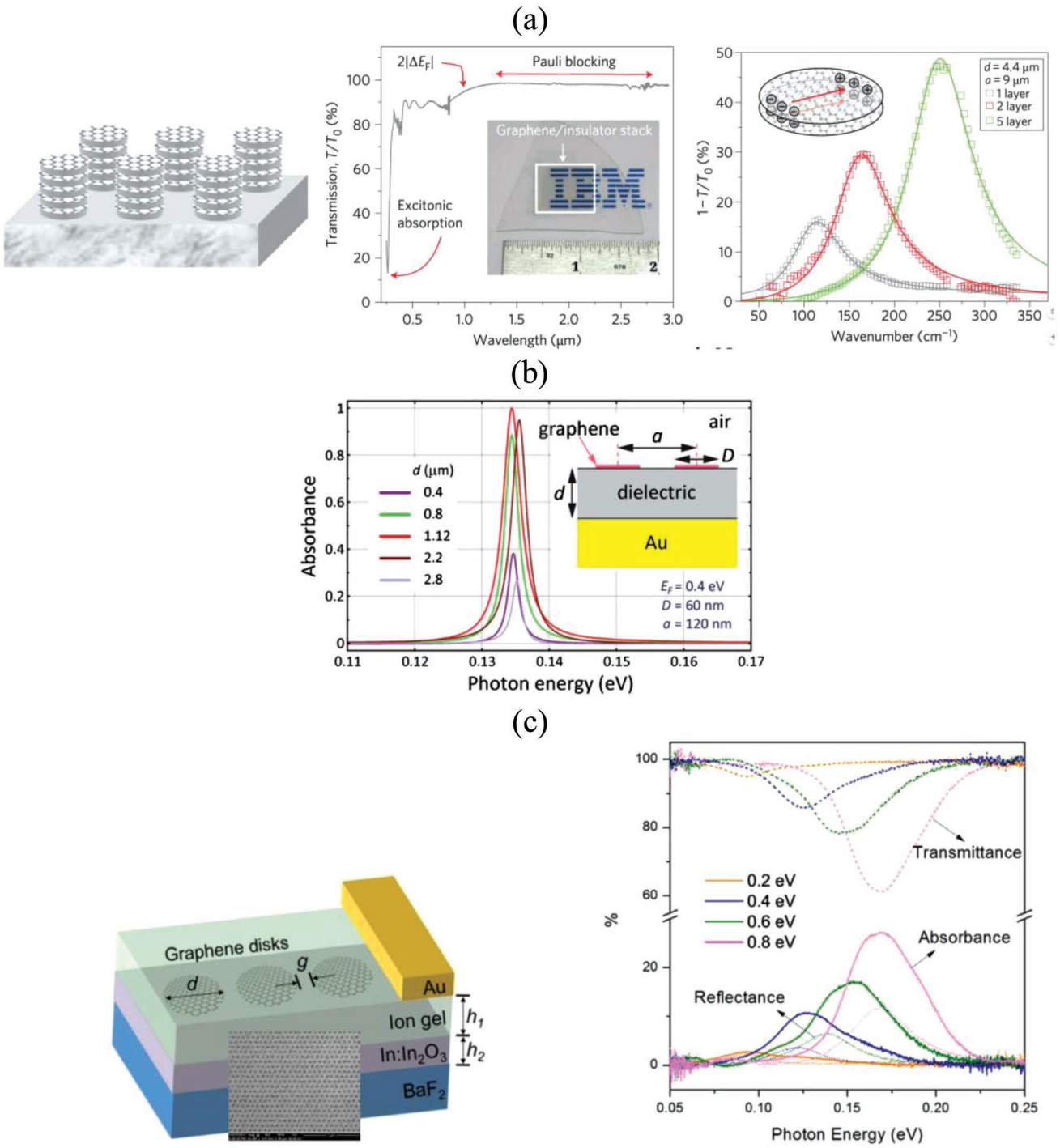


**Figure 8.** Patterned graphene structure. a) Schematic (left), transmission spectra (middle) in the NIR-visible region, and extinction spectra (right) in the far-infrared region of a device consisting of a stacked graphene/insulator microdisk array. Adapted with permission.[73] Copyright 2012, Springer Nature. b) Theoretical near total absorption by graphene disks. The colored lines are for various values of the dielectric film thickness. Adapted with permission.[35] Copyright 2012, APS. c) Left: Schematic, SEM image and absorbance of a graphene disk array configuration. Right: Measured transmittance, reflectance, and absorbance with Fermi energy ranging from 0.2 to 0.8 eV. Adapted with permission.[36] Copyright 2013, ACS.

even with a geometrically symmetric structure. Liu et al.[84] theoretically investigated localized surface-plasmon resonances in an array of monolayer BP nanoribbons placed on a dielectric spacer and an Au back reflector (**Figure 10**a,b), and observed anisotropic absorption spectrum along the armchair and zigzag directions of the BP monolayer, respectively. The calculated maximum absorption is 47% at the wavelength near 40 μm. Xiong et al.[85] numerically showed that

**Table 1.** Summary of absorption enhancement of graphene in the literature.

| Structure | Wavelength | Total absorption [%] | | Absorption in graphene [%] | | Bandwidth | No. of layers | References | Notes |
|---|---|---|---|---|---|---|---|---|---|
| | | Calculation | Experiment | Calculation | Experiment | | | | |
| With single mirrors | 550 nm | — | — | 9<br>≈24 | — | ≈110 nm | Single<br>Three | [58] | |
| | ≈13 µm | ≈100 | 77.6 | — | 47.2 | ≈1 µm | Single | [52] | At 89° angle-of-incidence* |
| With double mirrors | 855 nm | 98 | 60 | 98 | >54 | 9 nm | Single | [53] | * |
| | 1553 nm | 100 | — | 80 | — | ≈17 nm | Single | [62] | |
| With photonic crystals | ≈1590 nm | — | — | 50 | 16 | 26.8 nm | Single | [63] | |
| | 1545.5 nm | 39 | ≈35 | 39 | ≈35 | ≈4 nm | Single | [54] | * |
| | 737 nm | 60 | 43 | 60 | 43 | 7 nm | Single | [64] | * |
| | ≈1300 nm | 100 | — | 100 | — | 6 nm | Single | [65] | |
| With photonic crystals and back reflectors | 1500 nm | 100 | — | 100 | — | 14 nm | Single | [67] | |
| | 1545.5 nm | 90 | 85 | 90 | 85 | ≈4 nm | Single | [54] | |
| | 1507 nm | 95 | 96 | 84.70 | 77 | ≈3 nm | Single | [68] | # |
| | ≈735 nm | ≈100 | 37 | | — | ≈5 nm | Single | [55] | |
| | 1500 nm | 100 | 98.8 | 89 | — | 20 nm | Single | [69] | |
| | 1526.5 nm | 100 | 99.4 | — | — | 18 nm | Single | [70] | |
| | ≈1500 nm | — | — | 43.1<br>85.7 | — | ≈240 nm | Single<br>Five | [57] | |
| | 8.5 µm | ≈100 | 94 | 94 | — | 1.4 µm | Single | [71] | |
| Patterned graphene with mirrors | ≈9 µm | 100 | — | — | — | 150 nm | Single | [35] | At 20–45° angle-of-incidence |
| | ≈6.9 µm | 100 | 30 | — | 30 | ≈2 µm | Single | [36] | * |
| | ≈7.2 µm | — | 96.9 | — | — | — | Single | [76] | |

*Absorption in graphene obtained by deducting the absorptions of the structures without graphene from the total absorptions.
#Absorption in graphene obtained by measuring the photocurrent.

with the excitation of localized surface-plasmon resonances in a nanopatterned monolayer BP (an array of monolayer BP nanosquares), anisotropic perfect absorption can be realized. For the structure proposed therein (see Figure 10c,d), at the resonance wavelength of 22.8 µm, the total absorption for TM polarization (with the electric vector along the armchair direction) and TE polarization (with the electric vector along the zigzag direction) are 99.56% and 9.48%, respectively, resulting a polarization extinction ratio of over 23 dB. Such an anisotropic enhancement of absorption is purely due to the intrinsic material anisotropy, which can be further utilized to engineer a new class of anisotropic surface plasmons. For example, Huang et al.[86] experimentally revealed a new hybrid plasmon-phonon-polariton mode in a nanoribbon structure of black phosphorus carbide, which exhibits a strong anisotropic behavior, and can tuned through electrostatic doping (Figure 10e). This renders BP a more promising layered material for future optoelectronics.

**Table 2** summarizes the results from absorption enhancement of TMDs and BP described in this section. The table lists the structures, wavelengths, bandwidths, and magnitudes of absorption where reported.

## 5. Tunability of Enhanced Absorption in 2D Materials

In addition to the understanding of overall light interaction with the 2D materials, the potential of tunability is also important. Specifically, the Fermi levels of the 2D materials can be readily varied by applying an extra gate voltage (i.e., electrostatic doping),[1,87] contributing to change of electromagnetic properties, impedance matching, and surface plasmon resonance for the tunability of absorption. Absorption spectra of doped and suspended graphene were previously studied[25]; however, the effects of doping are not significant for creating tunable absorption devices. Nevertheless, localized surface plasmons in nanopatterned graphene can be dramatically tuned and hybridized through doping.[88] Therefore, nanopatterned graphene is favorable to the tunability of the enhanced absorption. Fang et al.[36] demonstrated that the absorption efficiency of an array of closely packed graphene nanodisks (see Figure 8b) can be electrically tuned from 2.6% to 27.8% (with the resonance wavelength changing from 15 to 7.4 µm) as the Fermi energy $E_F$ varied from 0.2 to 0.8 eV. Jang et al.[75] demonstrated that tunable resonant absorption can be achieved by varying doping

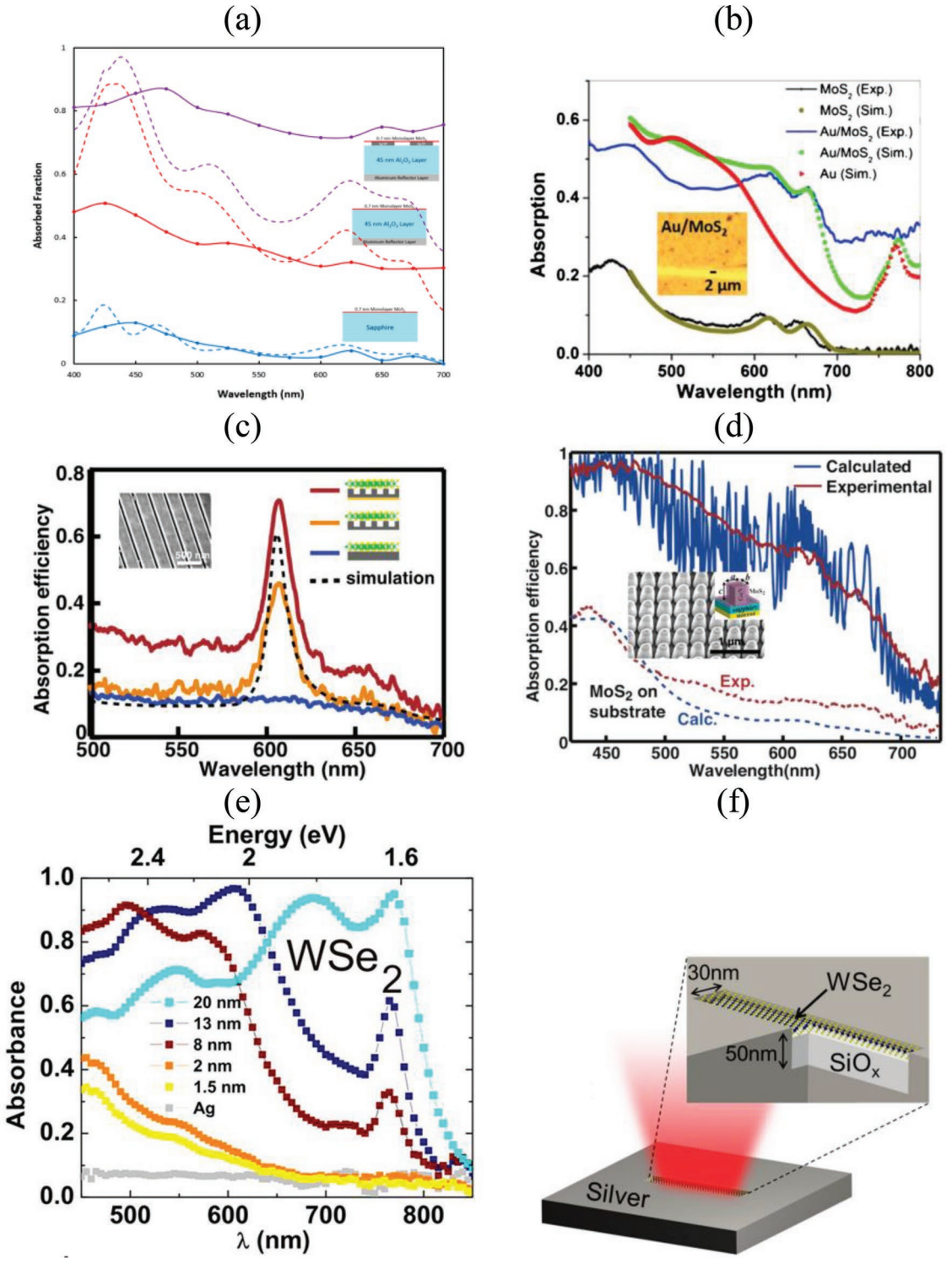


**Figure 9.** Schematics and absorbances of some TMD-based absorbers. a) Measured (solid lines) and simulated (dash lines) absorbance of $MoS_2$ monolayer on $Al_2O_3$ (blue), $Al_2O_3$/Al (red), and Ag NPs/$Al_2O_3$/Al (purple) substrates. Adapted with permission.[78] Copyright 2016, ACS. b) Absorbance of an Au NP-coated $MoS_2$. *Inset* is the optical image. Adapted with permission.[79] Copyright 2015, Springer Nature. c) Absorbance of an $MoS_2$ film on a GaN nanowire array (orange), on the GaN nanowire array with a back-coated mirror (red), and on a GaN unpatterned substrate (blue). *Inset* shows the SEM image of the GaN nanowire array. Adapted with permission.[56] Copyright 2016, ACS. d) Absorbance of a four-layer $MoS_2$ film coated on an array of GaN nanopillars (solid lines) and on an unpatterned substrate (dash lines). Adapted with permission.[56] Copyright 2016, ACS. e) Measured absorbance of $WSe_2$ flakes on an Ag back reflector. Colored lines are for various flake thickness. Adapted with permission.[80] Copyright 2016, ACS. f) Schematic of a $WSe_2$ monolayer emitter coupled to an optical slot antenna. Adapted with permission.[83] Copyright 2018, ACS.

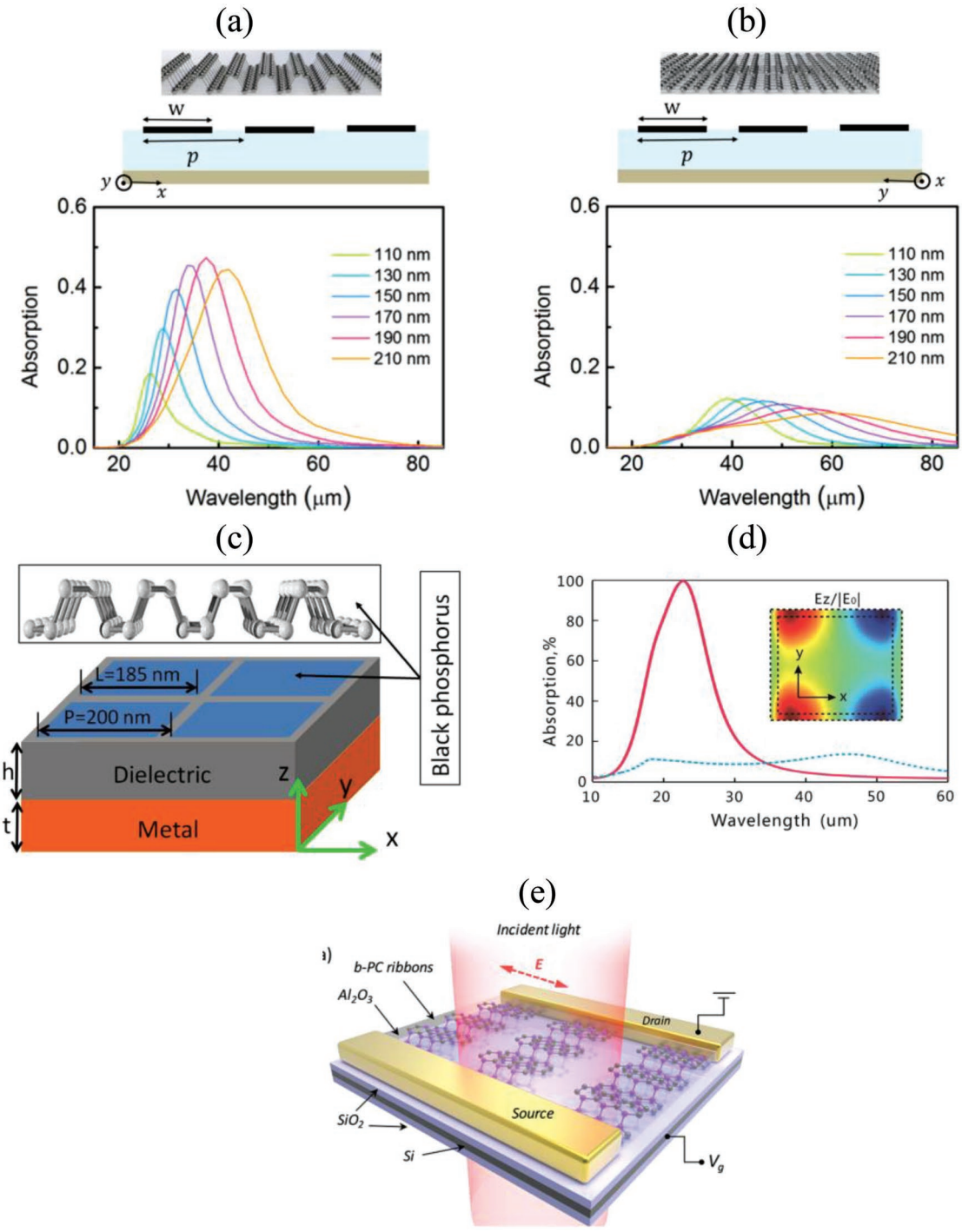


**Figure 10.** a,b) Schematics of absorbers consisting of BP ribbon arrays along (a) armchair direction and (b) zigzag direction, respectively, and the corresponding absorption spectra. Colored lines are for various widths of the BP ribbons. Adapted with permission.[84] Copyright 2016, ACS. c) Schematic of an absorber consisting of BP square array. d) Absorbance of the structure schemed in (c) for the electric vector along armchair (red solid line) and zigzag (blue dash line) direction. *Inset* shows the field distribution at the resonance wavelength. (c,d) Adapted with permission.[85] Copyright 2017, IOP Publishing Ltd. e) Schematic of a tunable anisotropic plasmonic b-PC metasurface. Adapted with permission.[86] Copyright 2018, ACS.

level in a nanopatterned graphene plasmonic metasurfaces (**Figure 11**a). The experimental total absorption in the graphene nanoresonators shows a large dependence on the graphene sheet carrier density, which varies from close to 0% to 24.5% as the carrier density is raised to $1.42 \times 10^{13}$ $cm^{-2}$ (Figure 11d). In another study, Kim et al.[76] demonstrated that 96.9% absorption in a graphene plasmonic nanostructure at 7.2 μm wavelength, with an on/off modulation efficiency of 95.9% in reflection (Figure 11d). The structure contains a single graphene ribbon surrounded by metallic strips (see Figure 11c).

**Table 2.** Summary of absorption enhancement of TMDs and BP in the literature.

| Structure | Material | Wavelength | Absorption efficiency [%] | Bandwidth | Layers | References |
|---|---|---|---|---|---|---|
| Films | $MoS_2$ | 0.66 μm | 34.9 | — | Single | [72] |
| | $MoS_2$ | 400–700 nm | 32 (avg.) | Broadband | Single | [78] |
| | $WSe_2$ | 500–600 nm | ≈100 | Broadband | 12–15 nm | [80] |
| | $MoS_2$ | 400–640 nm | 87 | Broadband | 14–18 nm | [81] |
| With photonic structures | $MoS_2$ | 600 nm | >70 | ≈40 nm | <4 layers | [56] |
| | $MoS_2$ | 400–690 nm | 51 (avg.) | Broadband | Single | [14] |
| | $MoS_2$ | 400–700 nm | >70 | Broadband | 4 layers | [56] |
| With plasmonic NPs | $MoS_2$ | 400–700 nm | 37 (avg.) | Broadband | Single | [78] |
| | $MoS_2$ | 400–800 nm | 41 (avg.) | Broadband | Single | [79] |
| Patterned | BP | 40 μm | 47 | ≈15 μm | Single | [84] |
| | BP | 22.8 μm | 99.56 | ≈10 μm | Single | [85] |

The metallic strips operate as mirrors for the graphene ribbon, which mimics a graphene plasmonic ribbon array and hence enables efficient absorption and modulation.

As for TMD monolayers, Yu et al.[89] reported that using electrical gating, the refractive index can be tuned by >60% in the imaginary part and >20% in the real part around exciton resonances, due to the effects of injected charge carriers to broaden the spectral width of excitonic interband transitions and to facilitate the interconversion of neutral and charged excitons. Based on such a giant tunability of refractive index, absorption in a TMD monolayer can be tuned from 40% to 80%, when combined with photonic structures (Figure 11e,f).

A summary of tunable enhanced absorption in the literature is tabulated in **Table 3**, which contains the tuning variables (the Fermi level and carrier density) and tuning ranges of wavelength and peak absorption.

## 6. Applications

Large enhancement and tunability of absorption in 2D materials is promising for new ultra-thin optoelectronic devices that interact with light, such as photodetectors,[90–92] photovoltaics,[93,94] and others. In principal, cavity- and plasmonic-based narrowband absorbers can be useful in filtering and sensing applications, while broadband enhancement of absorption in light trapping in thin-film solar cells. Practical applications are still in a very early stage of development. Here we outline a few potential applications as future directions.

### 6.1. Ultrafast, Responsive, and Chip-Integrated Photodetectors and Sensors

Graphene offers high tunability of carrier type and density (e.g., by electromagnetic gating, or chemical doping) as well as remarkable carrier mobility, which make it an ideal candidate in ultrafast detecting and sensing applications. The enhancement of light absorption in graphene, which is closely related to photocurrent enhancement in graphene-based devices,[95] is also essential for building photoresponsive devices since the 2.3% absorption in intrinsic graphene is far below what is needed. Examples of various graphene-based photodetectors have been reported, for example, electrostatically gate-controlled graphene photodetectors,[96,97] and graphene/Si Schottky diodes.[98–100] An example of graphene photodetectors incorporating cavity-coupled enhanced absorption was reported by Shiue et al.[101] By coupling to slow light modes in a long photonic crystal linear defect cavity (**Figure 12**a), they demonstrated controlled enhancement of photoresponsivity in the graphene photodetector, with an 8-fold enhancement of photocurrent at the resonant wavelength of 1535 nm (Figure 12b).

Light absorption, as well as light-matter interactions, can be significantly enhanced when photodetectors are combined with plasmonic nanostructures. Li et al.[102] demonstrated that high photoresponsivity is possible through the formation of so-called interfacial charge-transfer transition enabled by the intimate interfacing of metal and $MoS_2$. By taking advantage of the direct and intimate atomic contact of Au and $MoS_2$ in the Au@$MoS_2$ core-shell heterostructures, they realized an Au@$MoS_2$ heterojunction photodiode with a high photoresponsivity of 22.3 A/W (Figure 12c). Sourav et al.[103] reported a $MoS_2$-based plasmonic photodetector, which consists of a CVD-grown multilayer $MoS_2$ film and a split bull eye Al structure (Figure 12d). The plasmon-induced resonance helps to achieve six times enhancement of responsivity, compared to the reference device without the plasmonic structure.

The performance of the recent state-of-the-art 2D-material based photodetectors are not discussed here and can be found in other reviews.[104–106]

### 6.2. Controlled Thermal Light Emission

As outlined in Sections 4 and 5 the optical confinement enabled by micro- and nano-cavities can greatly enhance the magnitude and spectral selection of light absorption of monolayer graphene (and other 2D materials). On the other hand, the easy tuning of the Fermi energy and the density of states of graphene enables flexible electrical transport and heating with external sources. The combination of the two enables many possibilities of new functional devices, such as spectral sensitive and directional light modulators and emitters.[107,108] For example, Engel et al.[109] first showed that an electrically

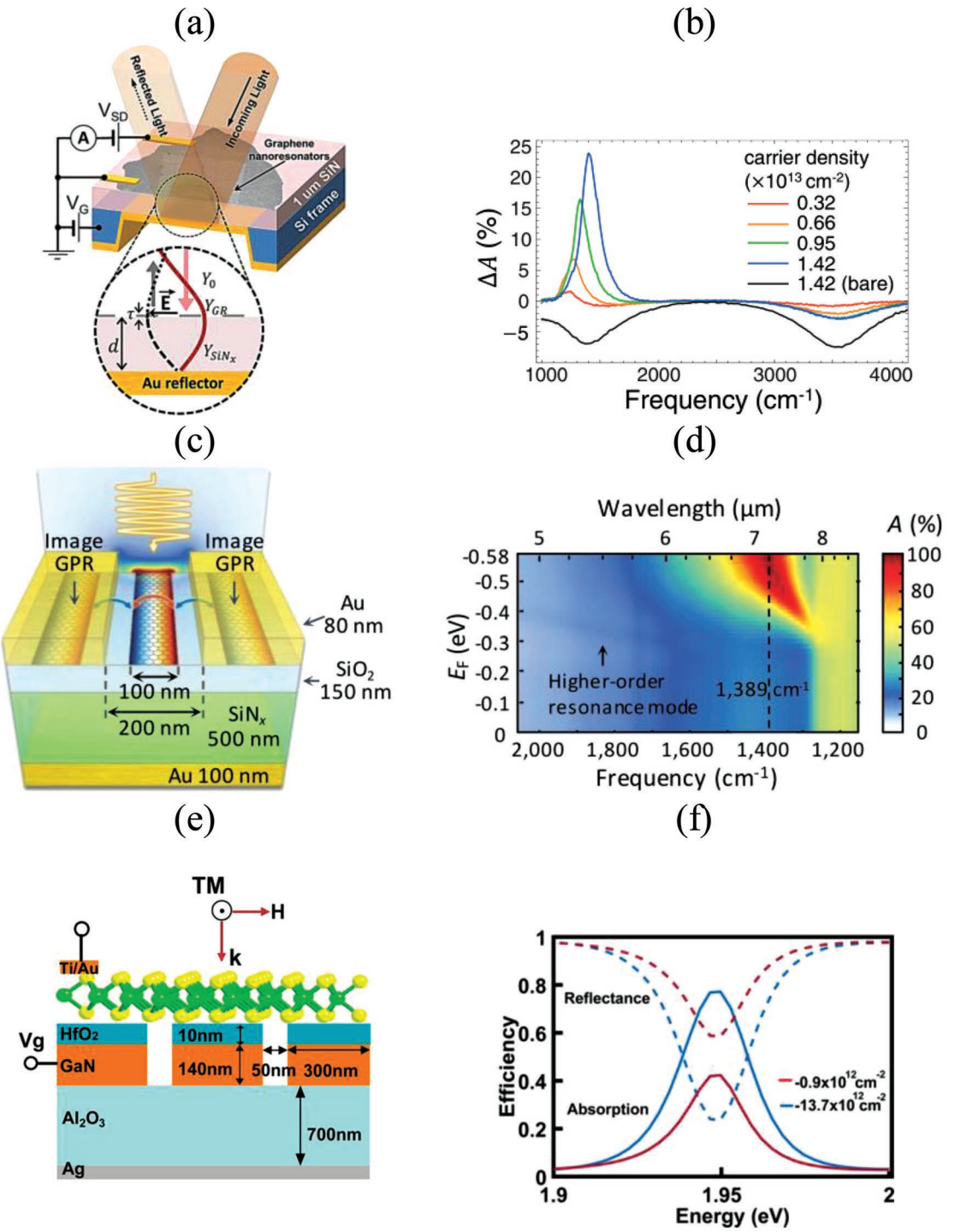


**Figure 11.** Electrically tunability of some 2D material absorbers. a) Schematic of a Salisbury screen configuration with a patterned graphene. *Inset* illustrates the device with the optical waves at the resonance condition. b) Change in absorption at various doping level. (a,b) Adapted with permission.[75] Copyright 2014, APS. c) Schematic of a structure containing a single graphene ribbon. d) Experimental gate-voltage dependent absorbance. (c,d) Adapted with permission.[76] Copyright 2018, ACS. e) Schematic of a gate tunable $WS_2$ absorber. f) Simulated absorption efficiency (solid line) and reflectance (dashed line) correspond to different electron injections induced by gate voltages. (e,f) Adapted with permission.[89] Copyright 2017, ACS.

contacted monolayer graphene, embedded in a planar microcavity, can act as a spectrally selective photodetector, and an electrically driven light emitter (**Figure 13**a). The cavity-induced light confinement not only controls the efficiency and spectral selection of photocurrent generation, but also the spectral properties of the electrically excited thermal radiation, as well as the electrical transport characteristics of the integrated graphene transistor (Figure 13b).

**Table 3.** Summary of tunable enhanced absorption in the literature.

| Structure | Variable (Fermi level in eV, carrier density in $cm^{-2}$) | Wavelength | Peak absorption [%] | References |
|---|---|---|---|---|
| Patterned graphene | 0.2–0.8 eV | 15–7.4 μm | 2.6–27.8 | [36] |
| | $-0.32 \times 10^{13}$ to $-1.42 \times 10^{13}$ $cm^{-2}$ | 8–7 μm | 1.5–24 | [75] |
| | −0.568 to −0.262 eV | 7.2–7.7 μm | 96.9–24.8 | [76] |
| TMD monolayer | $-0.9 \times 10^{12}$ to $-13.7 \times 10^{12}$ $cm^{-2}$ | 635 nm | 40–80 | [89] |
| BP monolayer | $2 \times 10^{13}$ to $7 \times 10^{13}$ $cm^{-2}$ | 27.6–16.2 μm | 78.4–100 | [85] |

### 6.3. Enhanced Luminous Efficiency

The direct bandgap of TMDs and the high charge carrier mobility provide great integration in novel optoelectronic devices. However, compared to other direct bandgap semiconductors, the inherent low quantum efficiency has limited the use of monolayer TMDs in high-performance optoelectronic devices. The nanostructures that enhance light absorption in TMD materials[56,77–81,110,111] may also allow increased quantum efficiency, and thus enhance optical device performance. For example, Jeong et al.[112] studied the modulation of the photoluminescence intensity from monolayer $MoS_2$ placed on a $TiO_2$/metal substrate as functions of the $TiO_2$ thickness and surface morphology of the metal, and observed large enhancement of photoluminescence intensity (more than 22 times) for an Al substrate with a rough surface (Figure 13c,d). This work demonstrates that the principles used to enhance absorption are also applicable to optimize the performance of 2D material incorporated devices, such as LEDs and lasers.[113,114]

### 6.4. Strong Coupling between Photons and 2D Material Excitons

The light confinement mechanisms not only enable enhanced absorption and emission in 2D material structures, but also open up strong coupling between photons and 2D material excitons. Strong coupling is a distinct region of light–matter interaction, where exciton and cavity modes resonate with each other forming a hybrid light-mater quasiparticle known as exciton-polariton. It gives rise to profound phenomena such as vacuum Rabi splitting, Bose–Einstein condensates[115] and superfluidity,[116] and also holds a great potential for developing low-power active devices such as polariton LEDs and lasers,[117] single-photon switches,[118]

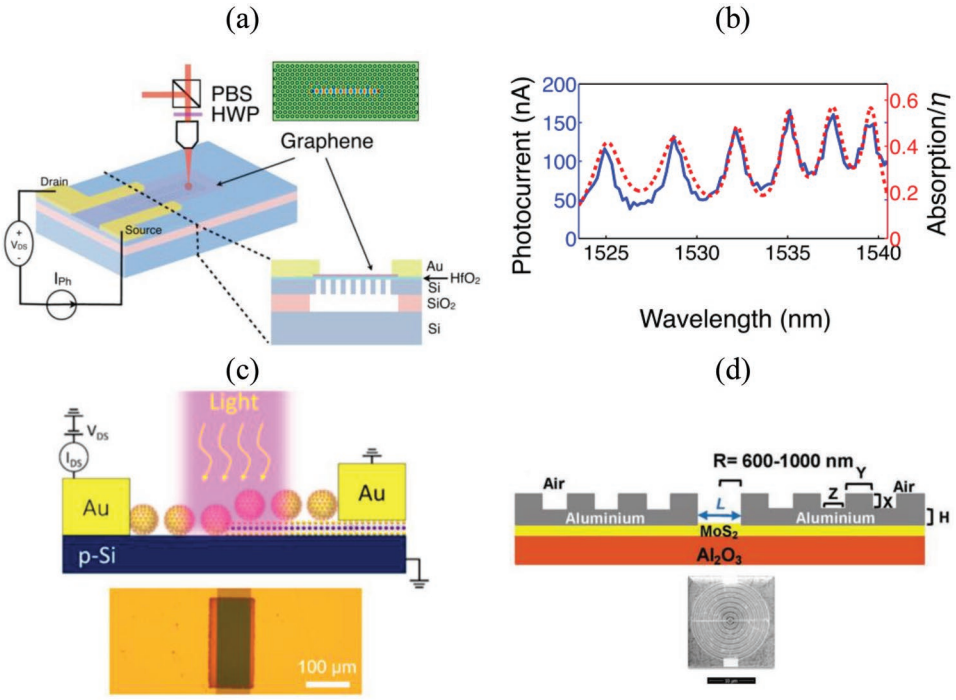


**Figure 12.** Enhanced photocurrent generation. a) Schematic of a planar PC cavity integrated graphene photodetector. The upper right inset shows a localized resonant mode inside the cavity. b) Photocurrent and absorption spectrum of the photodectector. (a,b) Adapted with permission.[101] Copyright 2013, AIP. c) Schematic and optical microscopic image of a high responsivity Au@$MoS_2$ photodiode. Adapted with permission.[102] Copyright 2017, ACS. d) Schematic and SEM image of a large-scale transparent $MoS_2$ photodetector. Reproduced with permission.[103] Copyright 2018, Wiley-VCH.

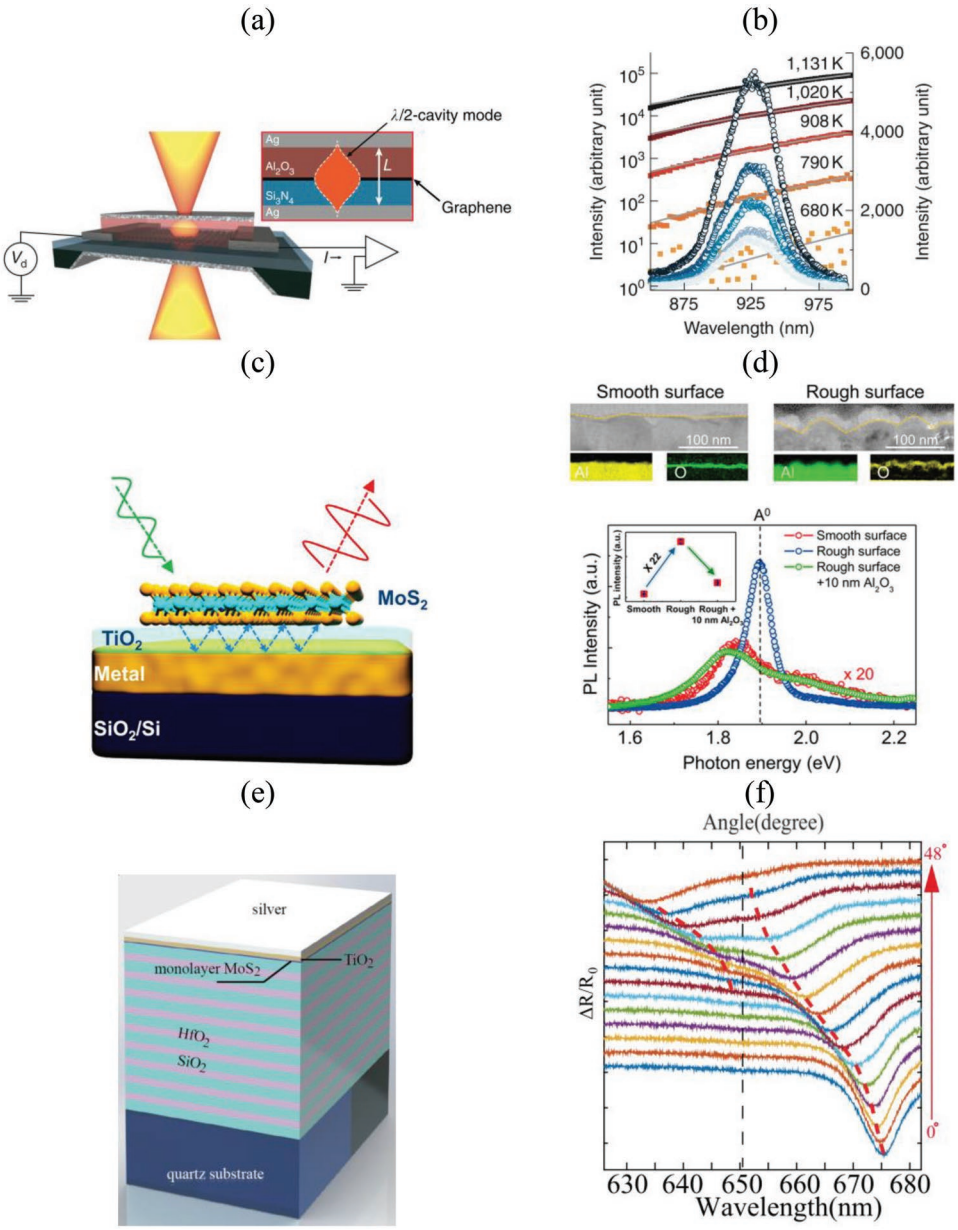


**Figure 13.** a) Schematic of a microcavity-controlled graphene thermal emitter. *Inset* is the cross-sectional view of the device. b) Near-infrared emission spectra for a cavity-confined (open circles, right *y*-axis) and a non-confined (filled squares, left *y*-axis) of the graphene emitter. (a,b) Adapted with permission.[109] Copyright 2012, Springer Nature. c,d) Enhanced photoluminescence (PL) intensity. c) Schematic of the photoluminescence of a $MoS_2$ monolayer on a metal film and a $TiO_2$ spacer. d) Top: Cross-sectional TEM images of smooth and rough surfaces of an Al film and EDX elemental mapping images for each case. Bottom: PL spectra of $MoS_2$ placed on a smooth (red) and rough (blue) Al surface and additional 10 nm thick $Al_2O_3$ film (green) on the rough Al surface. *Inset* shows the variation of the PL intensity at each step. (c,d) Adapted with permission.[112] Copyright 2016, American Chemical Society. e) Schematic of an exciton-polariton structure consisting of TPP cavity and monolayer $MoS_2$. f) Experimental of angle-resolved reflectivity spectra. (e,f) Adapted with permission.[121] Copyright 2017, AIP.

optical logic circuits. Experimentally strong coupling have been recognized between TMD material excitons and Fabry–Pérot structures[119–121] with Rabi splitting in absorption and fluorescence spectra. For example, Liu et al.[119] observed a Rabi splitting of 46 ± 3 meV in angle-resolved reflectivity and photoluminescence spectra. Their structure consists of a monolayer of $MoS_2$ and two $SiO_2/Si_3N_4$ distributed Bragg reflectors. The spectra show anti-crossing behavior and two prominent branches at room temperature, which are designated Rabi energy splitting for strong coupling. Similarly, Hu et al. demonstrated strong coupling between TPPs and the A excitons of monolayer $MoS_2$ with a Rabi splitting of 54 meV (Figure 13e,f). Compared with the previous work using distributed Bragg reflectors,[119] the use of the TPP modes gives a smaller mode volume, which is beneficial to the coupling strength.

## 7. Conclusions and Perspectives

We have described recent progress in enhancement of light absorptions in graphene and other 2D materials. Generally, 2D materials exhibit less than ideal absorption characteristics due to their atomically-thin thickness, limiting their deployment in practical optoelectronic applications. Therefore, absorption enhancement may be essential, and may be viewed as the first step to achieve high power conversion efficiency in designing a 2D-material-based optoelectronic device. Various designs, such as distributed Bragg reflector microcavities, metallic reflectors, PC nanocavities, and plasmonic nanostructures, have been designed to enhance light absorption and emission of 2D materials. To conclude the review, we tabulate in **Table 4** the advantages and disadvantages, as well as the application scopes of these structures.

Despite all the progress that has been made in enhancing the absorptions of the 2D materials, we would like to mention a few aspects of interest to this field, based on our own perspectives:

1. **Broadband and significant enhancement of absorption**. In the NIR-to-visible range there is still a need for broadband absorption enhancement. Normally, the resonator-coupled absorption structures, especially those with critically coupled designs, are highly narrowband, and one must trade between the bandwidth and amplitude of enhanced absorption. In principle broadband absorption can be done by utilizing multiple resonances, however, designing a micro- or nanocavity that can support multiple resonances with a significant overlap remains challenging.
2. **Turnabilities of enhanced absorption**. In the infra-to-THz range, by exploiting surface plasmon resonances, absorption in structures incorporating patterned and doped graphene can be effectively tuned with external electric fields. However, in the NIR-to-visible range, the absorption in graphene is dominated by interband transitions and can hardly be plasmon-enhanced, hence the turnabilities in this waveband is still less than favorable, and remains untouched.
3. **Challenges in fabrication**. The theoretical and experimental demonstrations of near-perfect absorption in 2D materials are encouraging, however, many factors in fabrication, such as complexity, fabrication tolerance, compatibility, and integrability with current optoelectrical devices, need to be further explored toward applicable 2D-material-based photonic devices.

Nevertheless, the absorption enhancement of atomically thin 2D materials may find its use in many optoelectronic applications. Critically coupled narrowband absorption enhancement in graphene may be utilized in sensing applications. TMDs have much higher absorption coefficient throughout the visible to near-infrared spectrum, and thus may find applications in ultra-thin high-efficiency solar cells. BP offers the potential for polarization-sensitive infrared detection due to its unique crystal structure. We anticipate the development will lead to many new opportunities for controlling light absorption in 2D materials, with possibilities for both fundamental advances and practical applications.

**Table 4.** Advantages, disadvantages, and applications of different 2D-material light absorption structures.

| Structures | Advantages | Disadvantages | Application scopes |
|---|---|---|---|
| Bare monolayer graphene | Broadband 2.3% absorption in NIR-to-visible region | | Infrared-to-visible |
| Bare monolayer TMDs | Broadband 10–30% absorption in visible region<br>Existence of exciton resonances | | Visible |
| Bare monolayer BP | Linear dichroism in IR-to-visible region | | Infrared |
| With a single mirror | • Simple<br>• Easy to fabricate | • Limited absorption enhancement<br>• Near-unity absorption only possible at a very large angle of incidence under critical coupling condition<br>• Parasitic absorption in metal if lossy metal is used as back reflector<br>• Relatively thick, less integratable | • Photodectors |
| With double mirrors | • Narrow, large absorption enhancement | • Narrowband<br>• Parasitic absorption in metal if lossy metal is used as back reflector<br>• Relatively thick, less integratable | |
| With PC/plasmonic nanocavities | • Narrow near-unity absorption<br>• Thin | • Narrowband<br>• Parasitic absorption in metal if lossy metal is used as back reflector or plasmonic structure | • Photodectors<br>• Optical modulators<br>• Chemical sensing and biosensing |
| Patterned plasmonic 2D materials | • Narrow near-unity absorption<br>• Excellent intensity and spectral tunability<br>• Reduced device thickness | • Narrowband<br>• Increased fabrication complexities | |
| TMDs/BP/metal heterostructures | • Broadband near-total absorption possible<br>• Direct photocurrent generation<br>• Ultrathin | • Increased fabrication complexities | • Photodectectors<br>• Light harvesting<br>• Photothermal applications |

## Acknowledgements

This work was supported by the National Key Research and Development Program of China (2017YFE0100200 and 2017YFA0205700) and the National Natural Science Foundation of China (Grant Nos. 61425023, 61575177, 61775194).

## Conflict of Interest

The authors declare no conflict of interest.

## Keywords

2D materials, graphene, light absorption

Received: April 10, 2019
Revised: June 10, 2019
Published online:

[1] K. S. Novoselov, A. K. Geim, S. V. Morozov, D. Jiang, Y. Zhang, S. V. Dubonos, I. V. Grigorieva, A. A. Firsov, *Science* **2004**, *306*, 666.
[2] A. K. Geim, *Science* **2009**, *324*, 1530.
[3] F. Xia, H. Wang, D. Xiao, M. Dubey, A. Ramasubramaniam, *Nat. Photonics* **2014**, *8*, 899.
[4] F. Bonaccorso, Z. Sun, T. Hasan, A. C. Ferrari, *Nat. Photonics* **2010**, *4*, 611.
[5] T. Mahmoudi, Y. Wang, Y.-B. Hahn, *Nano Energy* **2018**, *47*, 51.
[6] S. Z. Butler, S. M. Hollen, L. Cao, Y. Cui, J. A. Gupta, H. R. Gutiérrez, T. F. Heinz, S. S. Hong, J. Huang, A. F. Ismach, E. Johnston-Halperin, M. Kuno, V. V. Plashnitsa, R. D. Robinson, R. S. Ruoff, S. Salahuddin, J. Shan, L. Shi, M. G. Spencer, M. Terrones, W. Windl, J. E. Goldberger, *ACS Nano* **2013**, *7*, 2898.
[7] P. Chen, N. Li, X. Chen, W.-J. Ong, X. Zhao, *2D Mater.* **2018**, *5*, 014002.
[8] A. Ramasubramaniam, *Phys. Rev. B* **2012**, *86*, 115409.
[9] V. Tran, R. Soklaski, Y. Liang, L. Yang, *Phys. Rev. B* **2014**, *89*, 235319.
[10] L. Song, L. Ci, H. Lu, P. B. Sorokin, C. Jin, J. Ni, A. G. Kvashnin, D. G. Kvashnin, J. Lou, B. I. Yakobson, P. M. Ajayan, *Nano Lett.* **2010**, *10*, 3209.
[11] L. Britnell, R. M. Ribeiro, A. Eckmann, R. Jalil, B. D. Belle, A. Mishchenko, Y.-J. Kim, R. V. Gorbachev, T. Georgiou, S. V. Morozov, A. N. Grigorenko, A. K. Geim, C. Casiraghi, A. H. C. Neto, K. S. Novoselov, *Science* **2013**, *340*, 1311.
[12] W. J. Yu, Y. Liu, H. Zhou, A. Yin, Z. Li, Y. Huang, X. Duan, *Nat. Nanotechnol.* **2013**, *8*, 952.
[13] A. K. Geim, I. V. Grigorieva, *Nature* **2013**, *499*, 419.
[14] J. R. Piper, S. Fan, *ACS Photonics* **2016**, *3*, 571.
[15] J. Shim, H.-Y. Park, D.-H. Kang, J.-O. Kim, S.-H. Jo, Y. Park, J.-H. Park, *Adv. Electron. Mater.* **2017**, *3*, 1600364.
[16] A. K. Geim, K. S. Novoselov, *Nat. Mater.* **2007**, *6*, 183.
[17] R. R. Nair, P. Blake, A. N. Grigorenko, K. S. Novoselov, T. J. Booth, T. Stauber, N. M. R. Peres, A. K. Geim, *Science* **2008**, *320*, 1308.
[18] K. F. Mak, M. Y. Sfeir, Y. Wu, C. H. Lui, J. A. Misewich, T. F. Heinz, *Phys. Rev. Lett.* **2008**, *101*, 196405.
[19] M. Bruna, S. Borini, *Appl. Phys. Lett.* **2009**, *94*, 031901.
[20] F. J. Nelson, V. K. Kamineni, T. Zhang, E. S. Comfort, J. U. Lee, A. C. Diebold, *Appl. Phys. Lett.* **2010**, *97*, 253110.
[21] J. W. Weber, V. E. Calado, M. C. M. van de Sanden, *Appl. Phys. Lett.* **2010**, *97*, 091904.
[22] Q. Ye, J. Wang, Z. Liu, Z.-C. Deng, X.-T. Kong, F. Xing, X.-D. Chen, W.-Y. Zhou, C.-P. Zhang, J.-G. Tian, *Appl. Phys. Lett.* **2013**, *102*, 021912.
[23] S. Cheon, K. D. Kihm, H. Goo Kim, G. Lim, J. S. Park, J. S. Lee, *Sci. Rep.* **2015**, *4*, 6364.
[24] M. Klintenberg, S. Lebègue, C. Ortiz, B. Sanyal, J. Fransson, O. Eriksson, *J. Phys.: Condens. Matter* **2009**, *21*, 335502.
[25] L. Yang, *Nano Lett.* **2011**, *11*, 3844.
[26] P. Rani, G. S. Dubey, V. K. Jindal, *Phys. E* **2014**, *62*, 28.
[27] A. B. Kuzmenko, E. van Heumen, F. Carbone, D. van der Marel, *Phys. Rev. Lett.* **2008**, *100*, 117401.
[28] K. F. Mak, J. Shan, T. F. Heinz, *Phys. Rev. Lett.* **2011**, *106*, 046401.
[29] K. F. Mak, L. Ju, F. Wang, T. F. Heinz, *Solid State Commun.* **2012**, *152*, 1341.
[30] G. W. Hanson, *J. Appl. Phys.* **2008**, *103*, 064302.
[31] M. Amin, M. Farhat, H. Bağcı, *Sci. Rep.* **2013**, *3*, 2105.
[32] B. Sensale-Rodriguez, R. Yan, M. M. Kelly, T. Fang, K. Tahy, W. S. Hwang, D. Jena, L. Liu, H. G. Xing, *Nat. Commun.* **2012**, *3*, 780.
[33] A. Andryieuski, A. V. Lavrinenko, *Opt. Express* **2013**, *21*, 9144.
[34] O. Balci, E. O. Polat, N. Kakenov, C. Kocabas, *Nat. Commun.* **2015**, *6*, 6628.
[35] S. Thongrattanasiri, F. H. L. Koppens, F. J. García de Abajo, *Phys. Rev. Lett.* **2012**, *108*, 047401.
[36] Z. Fang, Y. Wang, A. E. Schlather, Z. Liu, P. M. Ajayan, F. J. García de Abajo, P. Nordlander, X. Zhu, N. J. Halas, *Nano Lett.* **2014**, *14*, 299.
[37] K. F. Mak, C. Lee, J. Hone, J. Shan, T. F. Heinz, *Phys. Rev. Lett.* **2010**, *105*, 136805.
[38] Y. Li, A. Chernikov, X. Zhang, A. Rigosi, H. M. Hill, A. M. van der Zande, D. A. Chenet, E.-M. Shih, J. Hone, T. F. Heinz, *Phys. Rev. B* **2014**, *90*, 205422.
[39] R. Kumar, I. Verzhbitskiy, G. Eda, *IEEE J. Quantum Electron.* **2015**, *51*, 1.
[40] Y. Yu, Y. Yu, Y. Cai, W. Li, A. Gurarslan, H. Peelaers, D. E. Aspnes, C. G. V. de Walle, N. V. Nguyen, Y.-W. Zhang, L. Cao, *Sci. Rep.* **2015**, *5*, 16996.
[41] T. Low, A. S. Rodin, A. Carvalho, Y. Jiang, H. Wang, F. Xia, A. H. Castro Neto, *Phys. Rev. B* **2014**, *90*, 075434.
[42] A. Castellanos-Gomez, L. Vicarelli, E. Prada, J. O. Island, K. L. Narasimha-Acharya, S. I. Blanter, D. J. Groenendijk, M. Buscema, G. A. Steele, J. V. Alvarez, H. W. Zandbergen, J. J. Palacios, H. S. J. van der Zant, *2D Mater.* **2014**, *1*, 025001.
[43] D. Li, H. Jussila, L. Karvonen, G. Ye, H. Lipsanen, X. Chen, Z. Sun, *Sci. Rep.* **2015**, *5*, 15899.
[44] S. Lan, S. Rodrigues, L. Kang, W. Cai, *ACS Photonics* **2016**, *3*, 1176.
[45] G. Zhang, S. Huang, A. Chaves, C. Song, V. O. Özçelik, T. Low, H. Yan, *Nat. Commun.* **2017**, *8*, 14071.
[46] L. Li, J. Kim, C. Jin, G. J. Ye, D. Y. Qiu, F. H. da Jornada, Z. Shi, L. Chen, Z. Zhang, F. Yang, K. Watanabe, T. Taniguchi, W. Ren, S. G. Louie, X. H. Chen, Y. Zhang, F. Wang, *Nat. Nanotechnol.* **2017**, *12*, 21.
[47] W. Wang, Y. Qu, K. Du, S. Bai, J. Tian, M. Pan, H. Ye, M. Qiu, Q. Li, *Appl. Phys. Lett.* **2017**, *110*, 101101.
[48] C. Manolatou, M. J. Khan, S. Fan, P. R. Villeneuve, H. A. Haus, J. D. Joannopoulos, *IEEE J. Quantum Electron.* **1999**, *35*, 1322.
[49] S. Fan, W. Suh, J. D. Joannopoulos, *J. Opt. Soc. Am. A* **2003**, *20*, 569.
[50] Q. Li, T. Wang, Y. Su, M. Yan, M. Qiu, *Opt. Express* **2010**, *18*, 8367.
[51] K.-K. Du, Q. Li, Y.-B. Lyu, J.-C. Ding, Y. Lu, Z.-Y. Cheng, M. Qiu, *Light: Sci. Appl.* **2017**, *6*, e16194.
[52] L. Zhu, F. Liu, H. Lin, J. Hu, Z. Yu, X. Wang, S. Fan, *Light: Sci. Appl.* **2016**, *5*, e16052.

[53] M. Furchi, A. Urich, A. Pospischil, G. Lilley, K. Unterrainer, H. Detz, P. Klang, A. M. Andrews, W. Schrenk, G. Strasser, T. Mueller, *Nano Lett.* **2012**, *12*, 2773.
[54] Y. Liu, A. Chadha, D. Zhao, J. R. Piper, Y. Jia, Y. Shuai, L. Menon, H. Yang, Z. Ma, S. Fan, F. Xia, W. Zhou, *Appl. Phys. Lett.* **2014**, *105*, 181105.
[55] M. Grande, M. A. Vincenti, T. Stomeo, G. V. Bianco, D. de Ceglia, N. Aközbek, V. Petruzzelli, G. Bruno, M. D. Vittorio, M. Scalora, A. D'Orazio, *Opt. Express* **2015**, *23*, 21032.
[56] L. Huang, G. Li, A. Gurarslan, Y. Yu, R. Kirste, W. Guo, J. Zhao, R. Collazo, Z. Sitar, G. N. Parsons, M. Kudenov, L. Cao, *ACS Nano* **2016**, *10*, 7493.
[57] H. Lu, B. P. Cumming, M. Gu, *Opt. Lett.* **2015**, *40*, 3647.
[58] J.-T. Liu, N.-H. Liu, J. Li, X. Jing Li, J.-H. Huang, *Appl. Phys. Lett.* **2012**, *101*, 052104.
[59] N. M. R. Peres, Y. V. Bludov, *EPL* **2013**, *101*, 58002.
[60] J.-T. Liu, N.-H. Liu, L. Wang, X.-H. Deng, F.-H. Su, *EPL* **2013**, *104*, 57002.
[61] G. Konstantatos, M. Badioli, L. Gaudreau, J. Osmond, M. Bernechea, F. P. G. de Arquer, F. Gatti, F. H. L. Koppens, *Nat. Nanotechnol.* **2012**, *7*, 363.
[62] H. Lu, X. Gan, B. Jia, D. Mao, J. Zhao, *Opt. Lett.* **2016**, *41*, 4743.
[63] M. G. Rybin, A. S. Pozharov, C. Chevalier, M. Garrigues, C. Seassal, R. Peretti, C. Jamois, P. Viktorovitch, E. D. Obraztsova, *Phys. Status Solidi B* **2012**, *249*, 2530.
[64] M. Grande, M. A. Vincenti, T. Stomeo, G. V. Bianco, D. de Ceglia, N. Aközbek, V. Petruzzelli, G. Bruno, M. D. Vittorio, M. Scalora, A. D'Orazio, *Opt. Express* **2014**, *22*, 31511.
[65] J. R. Piper, V. Liu, S. Fan, *Appl. Phys. Lett.* **2014**, *104*, 251110.
[66] J. Tian, H. Luo, Q. Li, X. Pei, K. Du, M. Qiu, *Laser Photonics Rev.* **2018**, *12*, 1800076.
[67] J. R. Piper, S. Fan, *ACS Photonics* **2014**, *1*, 347.
[68] W. Wang, A. Klots, Y. Yang, W. Li, I. I. Kravchenko, D. P. Briggs, K. I. Bolotin, J. Valentine, *Appl. Phys. Lett.* **2015**, *106*, 181104.
[69] C.-C. Guo, Z.-H. Zhu, X.-D. Yuan, W.-M. Ye, K. Liu, J.-F. Zhang, W. Xu, S.-Q. Qin, *Adv. Opt. Mater.* **2016**, *4*, 1955.
[70] Y. S. Fan, C. C. Guo, Z. H. Zhu, W. Xu, F. Wu, X. D. Yuan, S. Q. Qin, *Opt. Express* **2017**, *25*, 13079.
[71] I.-H. Lee, D. Yoo, P. Avouris, T. Low, S.-H. Oh, *Nat. Nanotechnol.* **2019**, *14*, 313.
[72] J.-T. Liu, T.-B. Wang, X.-J. Li, N.-H. Liu, *J. Appl. Phys.* **2014**, *115*, 193511.
[73] H. Yan, X. Li, B. Chandra, G. Tulevski, Y. Wu, M. Freitag, W. Zhu, P. Avouris, F. Xia, *Nat. Nanotechnol.* **2012**, *7*, 330.
[74] L. Ju, B. Geng, J. Horng, C. Girit, M. Martin, Z. Hao, H. A. Bechtel, X. Liang, A. Zettl, Y. R. Shen, F. Wang, *Nat. Nanotechnol.* **2011**, *6*, 630.
[75] M. S. Jang, V. W. Brar, M. C. Sherrott, J. J. Lopez, L. Kim, S. Kim, M. Choi, H. A. Atwater, *Phys. Rev. B* **2014**, *90*, 165409.
[76] S. Kim, M. S. Jang, V. W. Brar, K. W. Mauser, L. Kim, H. A. Atwater, *Nano Lett.* **2018**, *18*, 971.
[77] H. Lu, X. Gan, D. Mao, Y. Fan, D. Yang, J. Zhao, *Opt. Express* **2017**, *25*, 21630.
[78] S. M. Bahauddin, H. Robatjazi, I. Thomann, *ACS Photonics* **2016**, *3*, 853.
[79] B. Mukherjee, E. Simsek, *Plasmonics* **2016**, *11*, 285.
[80] D. Jariwala, A. R. Davoyan, G. Tagliabue, M. C. Sherrott, J. Wong, H. A. Atwater, *Nano Lett.* **2016**, *16*, 5482.
[81] Y. Zhang, W. Liu, Z. Li, H. Cheng, Y. Zhang, G. Jia, S. Chen, J. Tian, *Appl. Phys. Lett.* **2017**, *111*, 111109.
[82] S. Najmaei, A. Mlayah, A. Arbouet, C. Girard, J. Léotin, J. Lou, *ACS Nano* **2014**, *8*, 12682.
[83] M. S. Eggleston, S. B. Desai, K. Messer, S. A. Fortuna, S. Madhvapathy, J. Xiao, X. Zhang, E. Yablonovitch, A. Javey, M. C. Wu, *ACS Photonics* **2018**, *5*, 2701.
[84] Z. Liu, K. Aydin, *Nano Lett.* **2016**, *16*, 3457.
[85] F. Xiong, J. Zhang, Z. Zhu, X. Yuan, S. Qin, *J. Opt.* **2017**, *19*, 075002.
[86] X. Huang, Y. Cai, X. Feng, W. C. Tan, D. Md. N. Hasan, L. Chen, N. Chen, L. Wang, L. Huang, T. J. Duffin, C. A. Nijhuis, Y.-W. Zhang, C. Lee, K.-W. Ang, *ACS Photonics* **2018**, *5*, 3116.
[87] C.-F. Chen, C.-H. Park, B. W. Boudouris, J. Horng, B. Geng, C. Girit, A. Zettl, M. F. Crommie, R. A. Segalman, S. G. Louie, F. Wang, *Nature* **2011**, *471*, 617.
[88] Z. Fang, S. Thongrattanasiri, A. Schlather, Z. Liu, L. Ma, Y. Wang, P. M. Ajayan, P. Nordlander, N. J. Halas, F. J. García de Abajo, *ACS Nano* **2013**, *7*, 2388.
[89] Y. Yu, Y. Yu, L. Huang, H. Peng, L. Xiong, L. Cao, *Nano Lett.* **2017**, *17*, 3613.
[90] T. Mueller, F. Xia, P. Avouris, *Nat. Photonics* **2010**, *4*, 297.
[91] F. Xia, T. Mueller, Y. Lin, A. Valdes-Garcia, P. Avouris, *Nat. Nanotechnol.* **2009**, *4*, 839.
[92] S. Cakmakyapan, P. K. Lu, A. Navabi, M. Jarrahi, *Light: Sci. Appl.* **2018**, *7*, 20.
[93] D. M. Callahan, J. N. Munday, H. A. Atwater, *Nano Lett.* **2012**, *12*, 214.
[94] M. Bernardi, M. Palummo, J. C. Grossman, *Nano Lett.* **2013**, *13*, 3664.
[95] N. S. Mueller, S. Reich, *Phys. Rev. B* **2018**, *97*, 235417.
[96] M. C. Lemme, F. H. L. Koppens, A. L. Falk, M. S. Rudner, H. Park, L. S. Levitov, C. M. Marcus, *Nano Lett.* **2011**, *11*, 4134.
[97] N. M. Gabor, J. C. W. Song, Q. Ma, N. L. Nair, T. Taychatanapat, K. Watanabe, T. Taniguchi, L. S. Levitov, P. Jarillo-Herrero, *Science* **2011**, *334*, 648.
[98] C.-C. Chen, M. Aykol, C.-C. Chang, A. F. J. Levi, S. B. Cronin, *Nano Lett.* **2011**, *11*, 1863.
[99] H. Selvi, N. Unsuree, E. Whittaker, M. P. Halsall, E. W. Hill, A. Thomas, P. Parkinson, T. J. Echtermeyer, *Nanoscale* **2018**, *10*, 3399.
[100] X. An, F. Liu, Y. J. Jung, S. Kar, *Nano Lett.* **2013**, *13*, 909.
[101] R.-J. Shiue, X. Gan, Y. Gao, L. Li, X. Yao, A. Szep, D. Walker, J. Hone, D. Englund, *Appl. Phys. Lett.* **2013**, *103*, 241109.
[102] Y. Li, J. G. DiStefano, A. A. Murthy, J. D. Cain, E. D. Hanson, Q. Li, F. C. Castro, X. Chen, V. P. Dravid, *ACS Nano* **2017**, *11*, 10321.
[103] A. Sourav, Z. Li, Z. Huang, V. D. Botcha, C. Hu, J.-P. Ao, Y. Peng, H.-C. Kuo, J. Wu, X. Liu, K.-W. Ang, *Adv. Opt. Mater.* **2018**, *6*, 1800461.
[104] M. Long, P. Wang, H. Fang, W. Hu, *Adv. Funct. Mater.* **2019**, *29*, 1803807.
[105] J. Cheng, C. Wang, X. Zou, L. Liao, *Adv. Opt. Mater.* **2019**, *7*, 1800441.
[106] A. Rogalski, *Adv. Opt. Photonics* **2019**, *11*, 314.
[107] Y. Qu, Q. Li, K. Du, L. Cai, J. Lu, M. Qiu, *Laser Photonics Rev.* **2017**, *11*, 1700091.
[108] Y. Qu, Q. Li, L. Cai, M. Pan, P. Ghosh, K. Du, M. Qiu, *Light: Sci. Appl.* **2018**, *7*, 26.
[109] M. Engel, M. Steiner, A. Lombardo, A. C. Ferrari, H. v. Löhneysen, P. Avouris, R. Krupke, *Nat. Commun.* **2012**, *3*, 906.
[110] D. Huo, J. Zhang, H. Wang, X. Ren, C. Wang, H. Su, H. Zhao, *Nanoscale Res. Lett.* **2017**, *12*, 465.
[111] C. Janisch, H. Song, C. Zhou, Z. Lin, A. L. Elías, D. Ji, M. Terrones, Q. Gan, Z. Liu, *2D Mater.* **2016**, *3*, 025017.
[112] H. Y. Jeong, U. J. Kim, H. Kim, G. H. Han, H. Lee, M. S. Kim, Y. Jin, T. H. Ly, S. Y. Lee, Y.-G. Roh, W.-J. Joo, S. W. Hwang, Y. Park, Y. H. Lee, *ACS Nano* **2016**, *10*, 8192.
[113] Q. Bao, H. Zhang, Y. Wang, Z. Ni, Y. Yan, Z. X. Shen, K. P. Loh, D. Y. Tang, *Adv. Funct. Mater.* **2009**, *19*, 3077.
[114] Z. Sun, T. Hasan, F. Torrisi, D. Popa, G. Privitera, F. Wang, F. Bonaccorso, D. M. Basko, A. C. Ferrari, *ACS Nano* **2010**, *4*, 803.
[115] R. Balili, V. Hartwell, D. Snoke, L. Pfeiffer, K. West, *Science* **2007**, *316*, 1007.

[116] A. Amo, J. Lefrère, S. Pigeon, C. Adrados, C. Ciuti, I. Carusotto, R. Houdré, E. Giacobino, A. Bramati, *Nat. Phys.* **2009**, *5*, 805.
[117] C. Schneider, A. Rahimi-Iman, N. Y. Kim, J. Fischer, I. G. Savenko, M. Amthor, M. Lermer, A. Wolf, L. Worschech, V. D. Kulakovskii, I. A. Shelykh, M. Kamp, S. Reitzenstein, A. Forchel, Y. Yamamoto, S. Höfling, *Nature* **2013**, *497*, 348.
[118] T. Volz, A. Reinhard, M. Winger, A. Badolato, K. J. Hennessy, E. L. Hu, A. Imamoğlu, *Nat. Photonics* **2012**, *6*, 605.
[119] X. Liu, T. Galfsky, Z. Sun, F. Xia, E. Lin, Y.-H. Lee, S. Kéna-Cohen, V. M. Menon, *Nat. Photonics* **2015**, *9*, 30.
[120] S. Dufferwiel, S. Schwarz, F. Withers, A. A. P. Trichet, F. Li, M. Sich, O. Del Pozo-Zamudio, C. Clark, A. Nalitov, D. D. Solnyshkov, G. Malpuech, K. S. Novoselov, J. M. Smith, M. S. Skolnick, D. N. Krizhanovskii, A. I. Tartakovskii, *Nat. Commun.* **2015**, *6*, 8579.
[121] T. Hu, Y. Wang, L. Wu, L. Zhang, Y. Shan, J. Lu, J. Wang, S. Luo, Z. Zhang, L. Liao, S. Wu, X. Shen, Z. Chen, *Appl. Phys. Lett.* **2017**, *110*, 051101.
[122] C. Hsu, R. Frisenda, R. Schmidt, A. Arora, S. M. Vasconcellos, R. Bratschitsch, H. S. J. der Zant, A. Castellanos-Gomez, *Adv. Opt. Mater.* **2019**, *7*, 1900239.

 